

A closed-form 3D shell solution for multilayered structures subjected to different load combinations

Original

A closed-form 3D shell solution for multilayered structures subjected to different load combinations / Brischetto, Salvatore. - In: AEROSPACE SCIENCE AND TECHNOLOGY. - ISSN 1270-9638. - 70:(2017), pp. 29-46.
[10.1016/j.ast.2017.07.040]

Availability:

This version is available at: 11583/2678791 since: 2020-06-04T00:25:40Z

Publisher:

Elsevier

Published

DOI:10.1016/j.ast.2017.07.040

Terms of use:

This article is made available under terms and conditions as specified in the corresponding bibliographic description in the repository

Publisher copyright

(Article begins on next page)

A closed-form 3D shell solution for multilayered structures subjected to different load combinations

Salvatore Brischetto*

Abstract

Multilayered composite and sandwich plates and shells are typical aerospace structures. They introduce complicating effects such as in-plane and transverse anisotropy which lead to zigzag forms of displacement and interlaminar continuity problems. The present closed-form 3D shell solution allows the static analysis of simply-supported cross-ply laminated and sandwich plates, cylinders and cylindrical/spherical shell panels subjected to different harmonic load types. It is possible to consider transverse normal and transverse shear loads simultaneously or separately applied at the top and at the bottom of the considered structure. The present work extends the previous exact 3D shell model developed for the static analysis of plates and shells in the case of transverse normal load applied at the top or at the bottom of the investigated structure. This new extension is still based on the 3D equilibrium equations written in general orthogonal curvilinear coordinates. The obtained system is solved using simply supported boundary conditions, harmonic forms for loads and displacements, a general layer wise approach and the exponential matrix method for the solution of the differential equations in z . However, the load boundary conditions introduced in the proposed shell model have been opportunely modified in order to allow the combination of different transverse normal and transverse shear loads applied at the external surfaces. The new proposed benchmarks fill the gap present in the literature where the proposed 3D exact models always use a transverse normal load applied at the external surfaces. The present paper investigates the zigzag effects, the interlaminar continuity, the equilibrium and compatibility conditions, the load boundary conditions, the symmetry characteristics, the thickness ratio effect and the 3D behavior in laminated and sandwich plates and shells in the case of different load applications. The new proposed benchmarks will be fundamental for the validation of those new refined 2D shell models which want to capture all these features for different load types.

Keywords: transverse shear and transverse normal loads, shells and plates, closed-form solution, multilayered structures, 3D model, layer-wise approach.

1 Introduction

The principal betterments in the construction of aircraft and spacecraft have been obtained using multilayered structures. Typical configurations include: isotropic layers, such as aluminum and titanium alloys, which could be stacked with other materials in multilayered structures; carbon fiber reinforced laminates where the fiber orientation of each lamina can be changed to obtain the opportune strength

*Corresponding author: Salvatore Brischetto, Department of Mechanical and Aerospace Engineering, Politecnico di Torino, corso Duca degli Abruzzi, 24, 10129 Torino, ITALY. tel: +39.011.090.6813, fax: +39.011.090.6899, e.mail: salvatore.brischetto@polito.it.

and stiffness for the requested application; sandwich structures embedding a core made of honeycomb or metallic foam and external skins which can be made of isotropic alloy layers or composite laminates (sandwich structures are lightweight with high bending stiffness) [1]- [3]. Described layers can be combined in different numbers and ways to fulfill several structural requirements. In different aerospace structural applications, the described multilayered structures appear as two-dimensional and they are called plates or shells. The use of advanced materials and multilayered configurations in aerospace structures have led to a significant increase in the study and development of opportune three-dimensional (3D) or refined two-dimensional (2D) plate and shell models. Advanced multilayered structures introduce new complicating effects which are not present in the isotropic one-layered plates and shells [1]- [3]. The possibility of including these effects in the developed theories is fundamental for a correct implementation of 3D or refined 2D plate/shell models. The main complicating effects connected with the use of multilayered structures are the in-plane anisotropy and the transverse anisotropy [4], [5]. High in-plane anisotropy is shown in laminated panels including anisotropic layers, these structures have different mechanical-physical properties in the in-plane directions. Moreover, multilayered composite structures have higher transverse shear/normal flexibility with respect to in-plane deformability. This in-plane anisotropy gives a coupling between shear and axial strains which leads to several complications in the solution procedure for the analysis of anisotropic structures [6]- [8]. A second complicating effect of multilayered plates and shells is the transverse anisotropy which leads to different mechanical-physical properties through the thickness direction. This discontinuity in terms of mechanical properties produces a displacement field which has a rapid change of the slope in the thickness direction in correspondence to each layer interface [6]- [8]. This characteristic is known as the zigzag form of the displacement field in the thickness direction. The zigzag form of displacements in multilayered structures can be evaluated by means of opportune layer-wise approaches [9] or including appropriate zigzag functions in the equivalent single layer models. In-plane stresses can be discontinuous through the interfaces between the several layers included in the multilayered structure. Transverse stresses must be continuous at each layer interface in order to fulfill the equilibrium conditions. Displacements must be continuous at each layer interface in order to fulfill the compatibility conditions. For these reasons, displacements and transverse shear/normal stresses are continuous functions in the thickness direction with discontinuous first derivatives in z in correspondence at each layer (zigzag effect). The fulfillment of all these described requirements is a crucial point in the development of appropriate 3D and refined 2D shell models for the analysis of multilayered structures [10].

For the reasons described above, the use of advanced multilayered configurations has introduced a great challenge for researchers involved in the development of 3D and refined 2D shell models for the analysis of modern structures used in the aerospace, aircraft, marine and automotive engineering areas. Efficient and correct shell models must be able to describe complicating effects such as in-plane and transverse anisotropy (zigzag effects and interlaminar continuity) and they must allow a correct description of load conditions. These models must be included in appropriate advanced tools able to evaluate fundamental information such as stress levels, failure indexes, progressive failure analyses, modal analyses and instability phenomena of multilayered structures. Such innovative tools for the analysis of advanced multilayered structures will allow the design and manufacturing of modern structures that will be safer, lighter and more efficient leading to an important advantage for the community and the environment [1]- [3]. The main limitations of the most important 3D models presented in the literature are two: they are usually developed for a determined geometry (plate or cylindrical shell or spherical shell) and they propose a restricted static analysis with a simple load configuration. The well-known 3D exact solution by Pagano [11]- [13] was developed for the static analysis of composite laminated and sandwich square and rectangular plates when they are subjected to an harmonic transverse normal load (cylindrical bending analysis has also been performed). Xu and Zhou [14] considered a 3D elastic numerical plate model for the analysis of functionally graded rectangular plates with variable thickness when subjected to a transverse normal load applied in harmonic form. Meyer-Piening [15] declared

that his elasticity solution for beams and plates was easy to be extended to shell geometries. However, the proposed results considered transverse normal loads applied to plate structures. The closed-form 3D plate solution by Demasi [16] was based on the mixed form of the Hooke law and it considered harmonic transverse normal loads which can be simultaneously applied at the external surfaces. The exact solution by Ren [17] was developed for the cylindrical bending analysis of composite laminated cylindrical shells when they were subjected to transverse normal loads. Three-dimensional elasticity solutions in [18] were obtained for finite length, cross-ply laminated simply supported cylinders subjected to transverse normal sinusoidal loads. The analytical solutions by Fan and Zhang [19], [20] were developed for the static analysis of thick and thin laminated spherical shells when subjected to harmonic transverse normal loads usually applied at the top surface. The analytical 3D solution developed by Soldatos and Ye [21] for cylinders can consider different types of harmonic loads using the adopted cylindrical reference system. The exact 3D solution by Fan and Ye [22] was developed for laminated composite plates subject to typical load conditions. The 3D exact solution by Kashtalyan [23] developed for the static analysis of one-layered functionally graded rectangular plates considered only the application of a transverse normal harmonic load at the top surface. The same methodology was extended by Kashtalyan and Menshykova [24] to sandwich plates with a functionally graded core without modifying the load conditions already used in the work [23]. Further interesting elasticity models considered the free frequency or dynamic analysis, few examples were the works [25]- [28] for plate geometries and the papers [29]- [31] for shell geometries. Remarkable works about the free vibration, dynamic and static analysis of plates and shells by means of numerical 3D methods are [32]- [37].

The present 3D exact shell model has been already developed for the free frequency analysis of one-layered plates and shells, multilayered composite and sandwich structures, single-layered and multilayered functionally graded flat and curved panels, single- and double-walled carbon nanotubes in [38]- [52]. The extension to static analysis has been performed in [53] for multilayered composite/sandwich plates and shells, and in [54] for one-layered and sandwich functionally graded plates and shells. In both cases, an harmonic transverse normal load has been applied at the top or at the bottom surface simply imposing the opportune load boundary conditions. The present paper modifies such a 3D shell model imposing different load boundary conditions in order to perform the static analysis of sandwich and laminated plates and shells when subjected to simultaneous or separated transverse shear and transverse normal loads at the external surfaces. In this way, the proposed 3D shell model will be as general as possible if compared with typical 3D exact solutions in the literature. The present model allows the analysis of several geometries (plates, cylinders, cylindrical shells and spherical shells), several materials and laminations (comprising laminates and sandwich structures) and different load conditions in the framework of the harmonic loads. All the 3D exact models found in the literature do not have this general capabilities. Major aircraft components (such as wings, fuselage and tails) are comprised of basic structural elements which are designed to take a specific type of load. For this reason, the possibility of a structural model which can include several load types could be fundamental. A typical example is the fuselage which can be loaded by small air loads, concentrated loads from wings and landing gears, pay loads and internal pressure due to the pressurization effects. In these cases, the fuselage skin is subjected to shear stresses, stringers or longerons are subjected to bending moments and axial forces, frames and bulkheads are designed for concentrated loads and to maintain the shape.

The proposed model is based on a layer-wise approach and on the 3D equilibrium equations written in general orthogonal curvilinear coordinates valid for plates and shells with constant radii of curvature. Closed form solutions are obtained considering simply supported boundary conditions and harmonic forms for displacements and loads. The partial differential equations in z have been solved by means of the exponential matrix method. This method has been successfully applied in the past by Messina [27] to develop an exact three-dimensional plate solution written in orthogonal rectilinear coordinates, by Soldatos and Ye [21] to write and solve the 3D equilibrium equations written in cylindrical coordinates for the free frequency analysis of laminated cylinders, and by Fan and Zhang [20] for a 3D shell solution

based on the 3D equilibrium equations written in general curvilinear orthogonal coordinates. However, the solution by Fan and Zhang [20] was less general than that here proposed because they used a different procedure (where the transverse stresses are also primary variables of the problem), and they investigated spherical shell panels or plates when subjected to transverse normal loads.

2 General closed-form 3D shell solution

The closed-form solution of the proposed general 3D shell model can be developed in the case of simply supported edges and harmonic forms for displacements, loads and stresses. The harmonic form for the three displacement components is:

$$u^k(\alpha, \beta, z) = U^k(z) \cos(\bar{\alpha}\alpha) \sin(\bar{\beta}\beta) , \quad (1)$$

$$v^k(\alpha, \beta, z) = V^k(z) \sin(\bar{\alpha}\alpha) \cos(\bar{\beta}\beta) , \quad (2)$$

$$w^k(\alpha, \beta, z) = W^k(z) \sin(\bar{\alpha}\alpha) \sin(\bar{\beta}\beta) . \quad (3)$$

The harmonic form for the three possible loads is:

$$p_\alpha^k(\alpha, \beta, z) = P_\alpha^k(z) \cos(\bar{\alpha}\alpha) \sin(\bar{\beta}\beta) , \quad (4)$$

$$p_\beta^k(\alpha, \beta, z) = P_\beta^k(z) \sin(\bar{\alpha}\alpha) \cos(\bar{\beta}\beta) , \quad (5)$$

$$p_z^k(\alpha, \beta, z) = P_z^k(z) \sin(\bar{\alpha}\alpha) \sin(\bar{\beta}\beta) . \quad (6)$$

The harmonic form for the six stress components can be written as:

$$\sigma_{\alpha\alpha}^k(\alpha, \beta, z) = \Sigma_{\alpha\alpha}^k(z) \sin(\bar{\alpha}\alpha) \sin(\bar{\beta}\beta) , \quad (7)$$

$$\sigma_{\beta\beta}^k(\alpha, \beta, z) = \Sigma_{\beta\beta}^k(z) \sin(\bar{\alpha}\alpha) \sin(\bar{\beta}\beta) , \quad (8)$$

$$\sigma_{zz}^k(\alpha, \beta, z) = \Sigma_{zz}^k(z) \sin(\bar{\alpha}\alpha) \sin(\bar{\beta}\beta) , \quad (9)$$

$$\sigma_{\beta z}^k(\alpha, \beta, z) = \Sigma_{\beta z}^k(z) \sin(\bar{\alpha}\alpha) \cos(\bar{\beta}\beta) , \quad (10)$$

$$\sigma_{\alpha z}^k(\alpha, \beta, z) = \Sigma_{\alpha z}^k(z) \cos(\bar{\alpha}\alpha) \sin(\bar{\beta}\beta) , \quad (11)$$

$$\sigma_{\alpha\beta}^k(\alpha, \beta, z) = \Sigma_{\alpha\beta}^k(z) \cos(\bar{\alpha}\alpha) \cos(\bar{\beta}\beta) . \quad (12)$$

Superscript k indicates the generic physical layer. (α, β, z) is the general orthogonal curvilinear reference system. U^k, V^k and W^k indicate the three displacement amplitudes along the three directions α, β and z , respectively. P_α^k, P_β^k and P_z^k indicate the three load amplitudes along the three directions α, β and z , respectively. $\Sigma_{\alpha\alpha}^k, \Sigma_{\beta\beta}^k, \Sigma_{zz}^k, \Sigma_{\beta z}^k, \Sigma_{\alpha z}^k$ and $\Sigma_{\alpha\beta}^k$ are the six stress amplitudes for the normal and shear components. Coefficients $\bar{\alpha} = \frac{m\pi}{a}$ and $\bar{\beta} = \frac{n\pi}{b}$ are evaluated by means of the half-wave numbers m and n and the shell dimensions a and b measured in α and β directions. Both half-wave numbers and dimensions are calculated in correspondence to the mid-surface Ω_0 of the shell structure. A three-dimensional shell has the mid surface Ω_0 which is equidistant from the top and the bottom surfaces. The distance between the top and bottom surfaces measured in a direction perpendicular to the surface Ω_0 is the total thickness h of the shell structure [55], [56]. Radii of curvature R_α and R_β are evaluated in α and β directions at the level of the reference mid-surface Ω_0 (for this reason they are defined as mean radii of curvature). Parametric quantities for shells with constant radii of curvature vary with continuity through the thickness direction:

$$H_\alpha = \left(1 + \frac{z}{R_\alpha}\right) = \left(1 + \frac{\tilde{z} - h/2}{R_\alpha}\right) , \quad H_\beta = \left(1 + \frac{z}{R_\beta}\right) = \left(1 + \frac{\tilde{z} - h/2}{R_\beta}\right) , \quad H_z = 1 , \quad (13)$$

H_α and H_β can depend on z (which goes from $-h/2$ to $+h/2$ and it is measured starting from Ω_0 surface) or on \tilde{z} coordinate (which goes from 0 to h and it is measured starting from the bottom surface) [57].

The simply supported boundary conditions for the investigated plates and shells can be written as:

$$w = v = 0, \sigma_{\alpha\alpha} = 0 \quad \text{for} \quad \alpha = 0, a, \quad (14)$$

$$w = u = 0, \sigma_{\beta\beta} = 0 \quad \text{for} \quad \beta = 0, b, \quad (15)$$

Eqs.(14) and (15) are automatically satisfied by means of the choice made for the harmonic forms in Eqs.(1)-(3) and (7)-(12). Proposed plates and shells can be loaded at the top and at the bottom in z , α and β directions imposing the following load conditions at the external surfaces:

$$\sigma_{zz} = p_z, \quad \sigma_{\alpha z} = p_\alpha, \quad \sigma_{\beta z} = p_\beta \quad \text{for} \quad z = -h/2, +h/2 \quad \text{or} \quad \tilde{z} = 0, h, \quad (16)$$

in the proposed model the loads p_z , p_α and p_β can be directly imposed in terms of transverse normal and transverse shear stresses acting at the top and at the bottom of the whole multilayered structure.

The proposed 3D shell model is based on the following general differential equilibrium equations written in general orthogonal curvilinear coordinates α , β and z and valid for multilayered spherical shells having constant mean radii of curvature R_α and R_β :

$$H_\beta \frac{\partial \sigma_{\alpha\alpha}^k}{\partial \alpha} + H_\alpha \frac{\partial \sigma_{\alpha\beta}^k}{\partial \beta} + H_\alpha H_\beta \frac{\partial \sigma_{\alpha z}^k}{\partial z} + \left(\frac{2H_\beta}{R_\alpha} + \frac{H_\alpha}{R_\beta} \right) \sigma_{\alpha z}^k = 0, \quad (17)$$

$$H_\beta \frac{\partial \sigma_{\alpha\beta}^k}{\partial \alpha} + H_\alpha \frac{\partial \sigma_{\beta\beta}^k}{\partial \beta} + H_\alpha H_\beta \frac{\partial \sigma_{\beta z}^k}{\partial z} + \left(\frac{2H_\alpha}{R_\beta} + \frac{H_\beta}{R_\alpha} \right) \sigma_{\beta z}^k = 0, \quad (18)$$

$$H_\beta \frac{\partial \sigma_{\alpha z}^k}{\partial \alpha} + H_\alpha \frac{\partial \sigma_{\beta z}^k}{\partial \beta} + H_\alpha H_\beta \frac{\partial \sigma_{zz}^k}{\partial z} - \frac{H_\beta}{R_\alpha} \sigma_{\alpha\alpha}^k - \frac{H_\alpha}{R_\beta} \sigma_{\beta\beta}^k + \left(\frac{H_\beta}{R_\alpha} + \frac{H_\alpha}{R_\beta} \right) \sigma_{zz}^k = 0, \quad (19)$$

the most general form of these equations in the case of shells having variable radii of curvature can be found in [58] and [59].

The index k goes from 1 to N_L and it indicates the physical layers. In order to calculate the parametric coefficients through the thickness (see Eq.(13)), each physical layer is divided in an opportune number of mathematical layers. Therefore, the total number of physical and mathematical layers is equal to M and the employed index is j which goes from 1 to M . This new index can be used in the already proposed Eqs.(1)-(19) and in the new ones which will be proposed in the next part. The compact form of geometrical equations for shells with constant radii of curvature is:

$$\epsilon^j = \Delta^j \mathbf{u}^j, \quad (20)$$

where the strain vector is $\epsilon^j = \{\epsilon_{\alpha\alpha}^j \epsilon_{\beta\beta}^j \epsilon_{zz}^j \gamma_{\beta z}^j \gamma_{\alpha z}^j \gamma_{\alpha\beta}^j\}^T$ and the displacement vector is $\mathbf{u}^j = \{u^j v^j w^j\}^T$. T means the transpose of a vector. The 6×3 matrix Δ^j is:

$$\Delta^j = \begin{bmatrix} \frac{1}{H_\alpha^j} \frac{\partial}{\partial \alpha} & 0 & \frac{1}{H_{\alpha_1}^j R_\alpha} \\ 0 & \frac{1}{H_\beta^j} \frac{\partial}{\partial \beta} & \frac{1}{H_{\beta_1}^j R_\beta} \\ 0 & 0 & \frac{\partial}{\partial z} \\ 0 & \frac{\partial}{\partial z} - \frac{1}{H_\beta^j R_\beta} & \frac{1}{H_\beta^j} \frac{\partial}{\partial \beta} \\ \frac{\partial}{\partial z} - \frac{1}{H_\alpha^j R_\alpha} & 0 & \frac{1}{H_\alpha^j} \frac{\partial}{\partial \alpha} \\ \frac{1}{H_\beta^j} \frac{\partial}{\partial \beta} & \frac{1}{H_\alpha^j} \frac{\partial}{\partial \alpha} & 0 \end{bmatrix}, \quad (21)$$

symbol ∂ indicates the partial derivatives made with respect to the coordinates α , β and z . Radii of curvature R_α and R_β are evaluated with respect to the mid-reference surface Ω_0 . Parametric coefficients H_α^j and H_β^j are calculated in the middle of each j very thin mathematical layer. Eqs.(20) and (21)

are written for the spherical shell case but they automatically degenerate in those for cylindrical shells and for plates when one of the two radii of curvature or both are infinite (which also means one of the two parametric coefficients or both equal 1). The constitutive equations in compact form for a generic mathematical j layer are:

$$\boldsymbol{\sigma}^j = \mathbf{C}^j \boldsymbol{\epsilon}^j, \quad (22)$$

where the stress vector is $\boldsymbol{\sigma}^j = \{\sigma_{\alpha\alpha}^j \sigma_{\beta\beta}^j \sigma_{zz}^j \sigma_{\beta z}^j \sigma_{\alpha z}^j \sigma_{\alpha\beta}^j\}^T$ and the strain vector is $\boldsymbol{\epsilon}^j = \{\epsilon_{\alpha\alpha}^j \epsilon_{\beta\beta}^j \epsilon_{zz}^j \gamma_{\beta z}^j \gamma_{\alpha z}^j \gamma_{\alpha\beta}^j\}^T$. The 6×6 elastic coefficient matrix \mathbf{C}^j written for the j mathematical layer and for the structural reference system (orthotropic angle θ equals 0° or 90° , which means elastic coefficients C_{16}^j , C_{26}^j , C_{36}^j and C_{45}^j equal zero to obtain the closed form solution) is:

$$\mathbf{C}^j = \begin{bmatrix} C_{11}^j & C_{12}^j & C_{13}^j & 0 & 0 & 0 \\ C_{12}^j & C_{22}^j & C_{23}^j & 0 & 0 & 0 \\ C_{13}^j & C_{23}^j & C_{33}^j & 0 & 0 & 0 \\ 0 & 0 & 0 & C_{44}^j & 0 & 0 \\ 0 & 0 & 0 & 0 & C_{55}^j & 0 \\ 0 & 0 & 0 & 0 & 0 & C_{66}^j \end{bmatrix}. \quad (23)$$

The closed form of the 3D equilibrium equations is obtained via the substitution of Eqs.(1)-(3) and (20)-(23) in the general form proposed in Eqs.(17)-(19):

$$\begin{aligned} & \left(-\frac{C_{55}^j H_\beta^j}{H_\alpha^j R_\alpha^2} - \frac{C_{55}^j}{R_\alpha R_\beta} - \bar{\alpha}^2 \frac{C_{11}^j H_\beta^j}{H_\alpha^j} - \bar{\beta}^2 \frac{C_{66}^j H_\alpha^j}{H_\beta^j} \right) U^j + \left(-\bar{\alpha} \bar{\beta} C_{12}^j - \bar{\alpha} \bar{\beta} C_{66}^j \right) V^j + \\ & \left(\bar{\alpha} \frac{C_{11}^j H_\beta^j}{H_\alpha^j R_\alpha} + \bar{\alpha} \frac{C_{12}^j}{R_\beta} + \bar{\alpha} \frac{C_{55}^j H_\beta^j}{H_\alpha^j R_\alpha} + \bar{\alpha} \frac{C_{55}^j}{R_\beta} \right) W^j + \left(\frac{C_{55}^j H_\beta^j}{R_\alpha} + \frac{C_{55}^j H_\alpha^j}{R_\beta} \right) U_{,z}^j + \left(\bar{\alpha} C_{13}^j H_\beta^j + \right. \\ & \left. \bar{\alpha} C_{55}^j H_\beta^j \right) W_{,z}^j + \left(C_{55}^j H_\alpha^j H_\beta^j \right) U_{,zz}^j = 0, \end{aligned} \quad (24)$$

$$\begin{aligned} & \left(-\bar{\alpha} \bar{\beta} C_{66}^j - \bar{\alpha} \bar{\beta} C_{12}^j \right) U^j + \left(-\frac{C_{44}^j H_\alpha^j}{H_\beta^j R_\beta^2} - \frac{C_{44}^j}{R_\alpha R_\beta} - \bar{\alpha}^2 \frac{C_{66}^j H_\beta^j}{H_\alpha^j} - \bar{\beta}^2 \frac{C_{22}^j H_\alpha^j}{H_\beta^j} \right) V^j + \\ & \left(\bar{\beta} \frac{C_{44}^j H_\alpha^j}{H_\beta^j R_\beta} + \bar{\beta} \frac{C_{44}^j}{R_\alpha} + \bar{\beta} \frac{C_{22}^j H_\alpha^j}{H_\beta^j R_\beta} + \bar{\beta} \frac{C_{12}^j}{R_\alpha} \right) W^j + \left(\frac{C_{44}^j H_\alpha^j}{R_\beta} + \frac{C_{44}^j H_\beta^j}{R_\alpha} \right) V_{,z}^j + \left(\bar{\beta} C_{44}^j H_\alpha^j + \right. \\ & \left. \bar{\beta} C_{23}^j H_\alpha^j \right) W_{,z}^j + \left(C_{44}^j H_\alpha^j H_\beta^j \right) V_{,zz}^j = 0, \end{aligned} \quad (25)$$

$$\begin{aligned} & \left(\bar{\alpha} \frac{C_{55}^j H_\beta^j}{H_\alpha^j R_\alpha} - \bar{\alpha} \frac{C_{13}^j}{R_\beta} + \bar{\alpha} \frac{C_{11}^j H_\beta^j}{H_\alpha^j R_\alpha} + \bar{\alpha} \frac{C_{12}^j}{R_\beta} \right) U^j + \left(\bar{\beta} \frac{C_{44}^j H_\alpha^j}{H_\beta^j R_\beta} - \bar{\beta} \frac{C_{23}^j}{R_\alpha} + \bar{\beta} \frac{C_{22}^j H_\alpha^j}{H_\beta^j R_\beta} + \bar{\beta} \frac{C_{12}^j}{R_\alpha} \right) V^j + \\ & \left(\frac{C_{13}^j}{R_\alpha R_\beta} + \frac{C_{23}^j}{R_\alpha R_\beta} - \frac{C_{11}^j H_\beta^j}{H_\alpha^j R_\alpha^2} - \frac{2C_{12}^j}{R_\alpha R_\beta} - \frac{C_{22}^j H_\alpha^j}{H_\beta^j R_\beta^2} - \bar{\alpha}^2 \frac{C_{55}^j H_\beta^j}{H_\alpha^j} - \bar{\beta}^2 \frac{C_{44}^j H_\alpha^j}{H_\beta^j} \right) W^j + \\ & \left(-\bar{\alpha} C_{55}^j H_\beta^j - \bar{\alpha} C_{13}^j H_\beta^j \right) U_{,z}^j + \left(-\bar{\beta} C_{44}^j H_\alpha^j - \bar{\beta} C_{23}^j H_\alpha^j \right) V_{,z}^j + \left(\frac{C_{33}^j H_\beta^j}{R_\alpha} + \frac{C_{33}^j H_\alpha^j}{R_\beta} \right) W_{,z}^j + \\ & \left(C_{33}^j H_\alpha^j H_\beta^j \right) W_{,zz}^j = 0. \end{aligned} \quad (26)$$

Eqs.(24)-(26) are a system of three second order partial differential relations in z . They represent a general 3D shell model because the equations are valid for spherical shells but they degenerate in the cases of cylindrical panels and plates simply imposing one radius of curvature or both radii of curvature equal infinite. The compact form of these equations has been proposed in [53] and [54]. The coefficients

are constant, even if shell geometries are considered, because the j mathematical layers have been introduced. The compact form of the second order differential equations in z proposed in Eqs.(24)-(26) are transformed in a system of first order differential equations in z simply redoubling the number of variables as suggested in [60]- [63]. Considering a generic j mathematical layer, this new compact system is:

$$\mathbf{D}^j \frac{\partial \mathbf{U}^j}{\partial \tilde{z}} = \mathbf{A}^j \mathbf{U}^j, \quad (27)$$

where $\frac{\partial \mathbf{U}^j}{\partial \tilde{z}} = \mathbf{U}^{j'}$ and $\mathbf{U}^j = [U^j \ V^j \ W^j \ U^{j'} \ V^{j'} \ W^{j'}]$. Coordinate \tilde{z} goes from 0 at the bottom to h at the top. This paper is focused on the imposition of the load boundary conditions in order to perform several benchmarks with different load combinations. For this reason, there are some missed detailed steps which can be found in past author's works about the static analysis including only a transverse normal load [53], [54]. The system of differential equations given in Eq.(27) is solved by means of the exponential matrix method [60]- [63]. This feature means:

$$\mathbf{D}^j \mathbf{U}^{j'} = \mathbf{A}^j \mathbf{U}^j, \quad (28)$$

$$\mathbf{U}^{j'} = \mathbf{D}^{j-1} \mathbf{A}^j \mathbf{U}^j, \quad (29)$$

$$\mathbf{U}^{j'} = \mathbf{A}^{j*} \mathbf{U}^j, \quad (30)$$

with $\mathbf{A}^{j*} = \mathbf{D}^{j-1} \mathbf{A}^j$. Matrices \mathbf{D}^j , \mathbf{A}^j and \mathbf{A}^{j*} are constant in each j layer of the plate or shell structure. The solution of Eq.(30) for shell can be written in accordance with [61] and [62] because the coefficients can be considered as constant:

$$\mathbf{U}^j(\tilde{z}^j) = \exp(\mathbf{A}^{j*} \tilde{z}^j) \mathbf{U}^j(0) \quad \text{with } \tilde{z}^j \in [0, h^j], \quad (31)$$

where \tilde{z}^j is the coordinate through the thickness of each j layer (its values are 0 at the bottom and h^j at the top). The exponential matrix can be written substituting $\tilde{z}^j = h^j$ for each j mathematical layer:

$$\mathbf{A}^{j**} = \exp(\mathbf{A}^{j*} h^j) = \mathbf{I} + \mathbf{A}^{j*} h^j + \frac{\mathbf{A}^{j*2}}{2!} h^{j2} + \frac{\mathbf{A}^{j*3}}{3!} h^{j3} + \dots + \frac{\mathbf{A}^{j*N}}{N!} h^{jN}, \quad (32)$$

where \mathbf{I} is the identity matrix having 6×6 dimension. In order to apply a layer-wise approach to the model, it is mandatory the imposition of interlaminar continuity for displacements (compatibility conditions) and for transverse normal/shear stresses (equilibrium conditions). In compact form, these conditions are:

$$u_b^j = u_t^{j-1}, \quad v_b^j = v_t^{j-1}, \quad w_b^j = w_t^{j-1}, \quad (33)$$

$$\sigma_{zzb}^j = \sigma_{zzt}^{j-1}, \quad \sigma_{azb}^j = \sigma_{azt}^{j-1}, \quad \sigma_{\beta zb}^j = \sigma_{\beta zt}^{j-1}, \quad (34)$$

displacement and transverse stress components at the top (t) of the $j-1$ layer must be equal to displacements and transverse stress components at the bottom (b) of the j layer.

Using the compatibility conditions in Eq.(33), the equilibrium conditions in Eq.(34) and the opportune expansion for the exponential matrix as proposed in Eq.(32), the final equations are:

$$\mathbf{B}^M(h^M) \mathbf{H}_m \mathbf{U}^1(0) = \mathbf{P}_t^M, \quad (35)$$

$$\mathbf{B}^1(0) \mathbf{U}^1(0) = \mathbf{P}_b^1, \quad (36)$$

with load amplitudes applied at the external surfaces given as:

$$\mathbf{P}_t^M = \begin{bmatrix} P_{zt}^M \\ P_{\beta t}^M \\ P_{\alpha t}^M \end{bmatrix}, \quad \mathbf{P}_b^1 = \begin{bmatrix} P_{zb}^1 \\ P_{\beta b}^1 \\ P_{\alpha b}^1 \end{bmatrix}, \quad (37)$$

where superscripts M and 1 indicate last layer and first layer, respectively. Subscripts t and b mean top and bottom of the considered layer, respectively. Matrices $\mathbf{B}^M(h^M)$ and $\mathbf{B}^1(0)$ contain all the geometrical and material data of the investigated structure for the top of the last layer and the bottom of the first layer, respectively. \mathbf{H}_m contains the compatibility and equilibrium conditions for each j layer and relative interfaces. As seen in Eq.(37), loads can be applied at the top of the last (M) layer in z , β and α directions and at the bottom of the first (1) layer in z , β and α directions. A general system can be written as:

$$\begin{bmatrix} \mathbf{B}^M(h^M) & \mathbf{H}_m \\ & \mathbf{B}^1(0) \end{bmatrix} \mathbf{U}^1(0) = \mathbf{P} , \quad (38)$$

where the 6×6 \mathbf{E} matrix is:

$$\mathbf{E} = \begin{bmatrix} \mathbf{B}^M(h^M) & \mathbf{H}_m \\ & \mathbf{B}^1(0) \end{bmatrix} , \quad (39)$$

and the 6×1 unknown vector $\mathbf{U}^1(0)$ and load vector \mathbf{P} are:

$$\mathbf{U}^1(0) = \begin{bmatrix} U^1(0) \\ V^1(0) \\ W^1(0) \\ U^{1'}(0) \\ V^{1'}(0) \\ W^{1'}(0) \end{bmatrix} , \quad \mathbf{P} = \begin{bmatrix} P_{zt}^M \\ P_{\beta t}^M \\ P_{\alpha t}^M \\ P_{zb}^1 \\ P_{\beta b}^1 \\ P_{\alpha b}^1 \end{bmatrix} . \quad (40)$$

The final linear algebraic system to be solved is:

$$\mathbf{E} \mathbf{U}^1(0) = \mathbf{P} . \quad (41)$$

The vector $\mathbf{U}^1(0)$ contains the three displacement amplitudes evaluated at the bottom of the first layer and the relative derivatives made with respect to the z coordinate. The vector \mathbf{P} contains all the possible load amplitudes which can be applied at the external surfaces. The solution is based on a layer-wise approach and the matrix \mathbf{E} has always 6×6 dimension, independently from the number of employed mathematical layers M . The solution has been implemented in an in-house academic software called *3DES* developed by the author in a Matlab environment. Only spherical panel equations have been implemented because cylindrical shell and plate equations can be obtained as particular cases. The load vector \mathbf{P} in Eq.(40) can assume several forms depending how the load boundary conditions in Eqs.(16) have been imposed. Possible conditions can be σ_{zz} and/or $\sigma_{\alpha z}$ and/or $\sigma_{\beta z}$ equal 0 or equal the opportune load value applied at the top and/or at the bottom of the whole structure. Using these considerations, several benchmarks can be proposed also including the five benchmarks discussed in the next section.

The unknown vector $\mathbf{U}^1(0)$ is calculated from the solution of the system in Eq.(41). Such a vector contains the three displacement components evaluated at the bottom of the structure and their relative derivatives made with respect to the z coordinate. These six values are evaluated at the bottom, the use of compatibility and equilibrium conditions in Eqs.(33) and (34) allows the 6×1 vector \mathbf{U} at each thickness coordinate z . Strain and stress vectors are calculated through the thickness z employing Eqs.(20)-(23). The implemented method is very accurate for the displacement calculation because it is based on a layer-wise approach. The calculation of strains is very accurate because in Eqs.(20) and (21) the derivatives of displacements with respect to α and β are exactly calculated deriving their harmonic forms, and the derivatives of displacements with respect to z are directly obtained from the solution of system in Eq.(41). This method can be considered as a sort of mixed method because the derivatives of displacements with respect to z have not been numerically calculated. Exact values of strains through the z direction in Eqs.(20) and (21) give correct values of stresses through z direction by means of Eqs.(22) and (23).

3 Results

The proposed 3D exact shell solution has been verified and validated in [38]- [52] for the free vibration analysis of one-layered and multilayered isotropic, orthotropic, composite, sandwich and functionally graded plates and shells and for single- and double-walled carbon nanotubes. Afterwards, this model has also been developed and confirmed for the static analysis of one-layered and multilayered plates and shells including classical layers (see work [53]) and functionally graded layers (see work [54]). These last two bending analyses only considered transverse normal loads applied in harmonic form at the top or at the bottom of the proposed structures. Several comparisons with other 3D solutions have been proposed in [38]- [52] in the case of free vibration analysis. The present model has been successfully compared with the 3D solution by Vel and Batra [25] and Srinivas et al. [26] in the case of square isotropic plates, with the 3D shell solution by Armenakas et al. [29] for the case of isotropic cylinders, with the 3D solution by Messina [27] for the case of multilayered composite plates, with the 3D solution by Huang [30] for the case of multilayered composite cylindrical and spherical shell panels, with the 3D solution by Li et al. [28] for the case of sandwich plates with external classical skins and internal FGM core, and with the 3D solution by Zahedinejad et al. [31] for the case of one-layered FGM cylindrical shell panels. Further comparisons with other 3D solutions have been proposed in [53] and [54] in the case of static analysis when transverse normal loads were applied separately at the top or at the bottom of the structures. The proposed 3D shell model has been compared with the 3D solution by Pagano [12] for the case of rectangular composite laminated plates and square sandwich plates, with the 3D solution by Ren [17] for the case of composite laminated cylindrical shell panels, with the 3D solution by Varadan and Bhaskar [18] for the case of composite laminated cylinders, with the 3D solution by Fan and Zhang [20] for the case of laminated composite spherical shell panels, with the 3D solution by Kashtalyan [23] for the case of one-layered FGM plates and with the 3D solution by Kashtalyan and Menshykova [24] for the case of sandwich plates with FGM core.

In all these comparisons, the present 3D exact shell model used an order $N=3$ for the exponential matrix expansion and $M=300$ mathematical layers for the correct description of the shell geometry (curvature effects through the thickness). The new results proposed in the present paper consider plate and shell structures subjected to different combinations of transverse normal and transverse shear loads which can be simultaneously applied at both the top and bottom external surfaces. This new model has been obtained opportunely modifying the load boundary conditions in the 3D model already proposed in [53] and [54]. Pratically, the load boundary conditions in terms of stresses $\sigma_{\alpha z}$, $\sigma_{\beta z}$ and σ_{zz} are opportunely rewritten depending on the load configuration imposed at the external surfaces of the proposed structures. The 3D equilibrium equations and the solution method do not change with respect to the cases proposed in [53] and [54] where transverse normal loads were applied at the top or at the bottom of the structures. For this reason, the choice of the parameters $N=3$ and $M=300$ is still valid for the new benchmarks here proposed obtained modifying the load boundary conditions. The dimension of the system to be solved is always 6×6 for any proposed N and M value (even if a layer-wise approach is employed). Each term of the 6×6 matrix becomes more complicated when M and N increase.

3.1 Proposed benchmarks

The five proposed new benchmarks are summarized in Figures 1-5. The first benchmark (B1) considers a square sandwich plate with isotropic skins subjected to a transverse normal harmonic load applied simultaneously at the top and at the bottom surfaces with opposite signs (see Figure 1). The second benchmark (B2) shows a rectangular sandwich plate embedding composite skins subjected to a transverse shear harmonic load in the α direction simultaneously applied at the top and at the bottom with opposite signs (see Figure 2). The third benchmark (B3) investigates a two-layered composite cylinder subjected to a transverse shear harmonic load in the β direction simultaneously applied at

the top and at the bottom with opposite signs (see Figure 3). The fourth benchmark (B4) proposes a three-layered composite cylindrical shell panel subjected to a transverse shear harmonic load applied in β direction at the top surface (see Figure 4). The last benchmark (B5) is devoted to the static analysis of a four-layered composite spherical shell panel where a transverse shear harmonic load is applied at the top surface in α direction (see Figure 5). Results for the five proposed benchmarks are given in terms of no-dimensional displacement and stress amplitudes calculated in different positions through the thickness direction. These results are shown in graphical form in Figures 6-11 and in tabular form in Tables 1-5. In the following five paragraphs, each benchmark is described in details and all the results are opportunely discussed remarking the main conclusions.

The first benchmark (B1 in Figure 1) proposes a simply supported square sandwich plate with isotropic skins. The transverse normal load is simultaneously applied at the top ($P_z^t = -1Pa$) and at the bottom ($P_z^b = 1Pa$) with half-wave numbers $m = n = 1$. The dimensions are $a = b = 1m$ with thickness ratios $a/h = 2, 4, 10, 20, 50, 100$. The two external skins have thickness values $h_1 = h_3 = 0.1h$ and the soft core has thickness $h_2 = 0.8h$ where h is the total thickness. The external skins are in Aluminum Alloy with Young Modulus $E = 73GPa$ and Poisson ratio $\nu = 0.3$ (isotropic material). The internal soft isotropic core has Young Modulus $E = 180MPa$ and Poisson ratio $\nu = 0.37$. $M = 300$ mathematical layers and order $N = 3$ for the exponential matrix are used. The no-dimensional displacements and stresses have the following form:

$$\{\bar{u}, \bar{v}, \bar{w}\} = \frac{10^2 E^{skin} \{u, v, w\}}{P_z^b h (a/h)^4}, \quad \{\bar{\sigma}_{\alpha\alpha}, \bar{\sigma}_{\beta\beta}, \bar{\sigma}_{\alpha\beta}\} = \frac{\{\sigma_{\alpha\alpha}, \sigma_{\beta\beta}, \sigma_{\alpha\beta}\}}{P_z^b (a/h)^2}, \quad (42)$$

$$\{\bar{\sigma}_{\alpha z}, \bar{\sigma}_{\beta z}\} = \frac{\{\sigma_{\alpha z}, \sigma_{\beta z}\}}{P_z^b (a/h)}, \quad \bar{\sigma}_{zz} = \sigma_{zz}.$$

Results in Table 1 propose the no-dimensional displacement and stress amplitudes through different thickness positions z for several thickness ratios (from very thick plates ($a/h=2$) to very thin plates ($a/h=100$)). New refined 2D models in the literature will be able to describe the 3D behavior of such a structure if they will propose results in accordance with those given in the present table. These results can be easily discussed using the first image of Figure 6 about the three displacement components for the thickness ratio $a/h=4$ and the Figure 7 for the six stress components for the thickness ratio $a/h=4$. Displacements \bar{u} , \bar{v} and \bar{w} in the first image of Figure 6 show the classical zigzag form which is typical of thick sandwich plates where the elastic properties of the skins are completely different from those of the core. The in-plane displacements \bar{u} and \bar{v} are coincident for symmetry reasons (square plate, isotropic materials and symmetrical load conditions). Moreover, the three displacement components are continuous at each interface skin-core because the compatibility conditions have been successfully imposed in the model. The normal in-plane and shear in-plane stresses $\bar{\sigma}_{\alpha\alpha}$, $\bar{\sigma}_{\beta\beta}$ and $\bar{\sigma}_{\alpha\beta}$ in Figure 7 are discontinuous at each interface skin-core and they show the typical behavior of sandwich structures. Transverse normal and transverse shear stresses $\bar{\sigma}_{zz}$, $\bar{\sigma}_{\alpha z}$ and $\bar{\sigma}_{\beta z}$ in Figure 7 are continuous through the thickness because the equilibrium conditions have been successfully imposed in the model. The $\bar{\sigma}_{zz}$ stress satisfies the load boundary conditions which mean $\bar{\sigma}_{zz}^t = P_z^t = -1Pa$ and $\bar{\sigma}_{zz}^b = P_z^b = +1Pa$. The $\bar{\sigma}_{\alpha z}$ and $\bar{\sigma}_{\beta z}$ stresses satisfy the load boundary conditions which are $\bar{\sigma}_{\alpha z}^t = P_\alpha^t = \bar{\sigma}_{\alpha z}^b = P_\alpha^b = 0Pa$ and $\bar{\sigma}_{\beta z}^t = P_\beta^t = \bar{\sigma}_{\beta z}^b = P_\beta^b = 0Pa$, respectively. Stresses $\bar{\sigma}_{\alpha z}$ and $\bar{\sigma}_{\beta z}$ are coincident because the plate is square, the layers are isotropic and the loads are applied in a symmetric way.

The second benchmark (B2 in Figure 2) includes a simply supported rectangular sandwich plate with composite skins. A transverse shear load is simultaneously applied at the top ($P_\alpha^t = 1Pa$) and at the bottom ($P_\alpha^b = -1Pa$) with half-wave numbers $m = n = 1$. The dimensions are $a = 1m$ and $b = 3m$ with thickness ratios $a/h = 2, 4, 10, 20, 50, 100$. The external skin at the bottom is made of two composite layers with thickness values $h_1 = h_2 = 0.05h$ and fibre orientation $0^\circ/90^\circ$. The top external skin embeds two composite layers with thickness values $h_4 = h_5 = 0.05h$ and fibre orientation $90^\circ/0^\circ$. The internal soft central core has the same elastic properties already proposed in the benchmark 1, the thickness

value is $h_3 = 0.8h$. The elastic properties of composite layers are Young moduli $E_1 = 132.38GPa$ and $E_2 = E_3 = 10.756GPa$, shear moduli $G_{12} = G_{13} = 5.6537GPa$ and $G_{23} = 3.603GPa$ and Poisson ratios $\nu_{12} = \nu_{13} = 0.24$ and $\nu_{23} = 0.49$. $M = 300$ mathematical layers and order $N = 3$ for the exponential matrix are used. The displacements and stresses have the following no-dimensional form:

$$\{\bar{u}, \bar{v}, \bar{w}\} = \frac{10^5 E_2^{skin} \{u, v, w\}}{P_\alpha^t h (a/h)^4}, \quad \{\bar{\sigma}_{\alpha\alpha}, \bar{\sigma}_{\beta\beta}, \bar{\sigma}_{\alpha\beta}\} = \frac{10^4 \{\sigma_{\alpha\alpha}, \sigma_{\beta\beta}, \sigma_{\alpha\beta}\}}{P_\alpha^t (a/h)^2}, \quad (43)$$

$$\{\bar{\sigma}_{zz}, \bar{\sigma}_{\beta z}\} = \frac{10^4 \{\sigma_{zz}, \sigma_{\beta z}\}}{P_\alpha^t (a/h)}, \quad \bar{\sigma}_{\alpha z} = \sigma_{\alpha z}.$$

Results in Table 2 show the no-dimensional displacement and stress amplitudes for different z values and for several thickness ratios (from very thick plates ($a/h=2$) to very thin plates ($a/h=100$)). New refined 2D models proposed in the literature will give a 3D description of such a structure if their results will be in accordance with those proposed in the present table. These results are given in graphical form in the second image of Figure 6 for the three displacement components for the thickness ratio $a/h=4$ and in the Figure 8 for the six stress components for the thickness ratio $a/h=4$. Displacements \bar{u} , \bar{v} and \bar{w} in the second image of Figure 6 show the classical zigzag form which is typical of thick sandwich plates where the elastic properties of the skins are completely different from those of the core. The differences with respect to the first case is due to the use of composite skins in place of isotropic skins. The in-plane displacements \bar{u} and \bar{v} have a different behavior through the thickness because the sandwich plate is now rectangular, it includes composite orthotropic skins and the load conditions are not symmetric. However, the three displacement components remain continuous at each interface skin-core and layer-layer in the skins because the compatibility conditions have been opportunely introduced in the model. The normal in-plane and shear in-plane stresses $\bar{\sigma}_{\alpha\alpha}$, $\bar{\sigma}_{\beta\beta}$ and $\bar{\sigma}_{\alpha\beta}$ in Figure 8 are discontinuous at each interface and they show the typical behavior of sandwich structures. In this case there are more discontinuity points because there are more interfaces (interfaces between skins and core, and interfaces between the two layers which constitute each external composite skin). Stresses $\bar{\sigma}_{\alpha\alpha}$ and $\bar{\sigma}_{\beta\beta}$ are different because there is not the symmetry in terms of geometry, material and load conditions. Transverse normal and transverse shear stresses $\bar{\sigma}_{zz}$, $\bar{\sigma}_{\alpha z}$ and $\bar{\sigma}_{\beta z}$ in Figure 8 are continuous through the thickness because the equilibrium conditions have been opportunely elaborated in the proposed 3D shell model. The $\bar{\sigma}_{zz}$ stress satisfies the load boundary conditions which mean $\bar{\sigma}_{zz}^t = \bar{\sigma}_{zz}^b = P_z^t = P_z^b = 0Pa$. The $\bar{\sigma}_{\alpha z}$ satisfies the load boundary conditions which are $\bar{\sigma}_{\alpha z}^t = P_\alpha^t = +1Pa$ and $\bar{\sigma}_{\alpha z}^b = P_\alpha^b = -1Pa$. The $\bar{\sigma}_{\beta z}$ stress satisfies the load boundary conditions which are $\bar{\sigma}_{\beta z}^t = \bar{\sigma}_{\beta z}^b = P_\beta^t = P_\beta^b = 0Pa$. Stresses $\bar{\sigma}_{\alpha z}$ and $\bar{\sigma}_{\beta z}$ are not coincident because the plate is rectangular, the layers for the skins are orthotropic and the load conditions are completely different for the two stress components.

The third benchmark (B3 in Figure 3) shows a simply supported composite cylinder. A transverse shear load is simultaneously applied at the top ($P_\beta^t = 1Pa$) and at the bottom ($P_\beta^b = -1Pa$) with half-wave numbers $m = n = 2$. The radii of curvature are $R_\alpha = 10m$ and $R_\beta = \infty$. The dimensions are $a = 2\pi R_\alpha$ and $b = 20m$. The two layers have thickness values $h_1 = h_2 = 0.5h$ with fiber orientation 0° for the first layer at the bottom and 90° for the second layer at the top. The investigated thickness ratios are $R_\alpha/h = 2, 4, 10, 50, 100, 500$. The elastic properties of the two composite layers are the same already seen in the second benchmark for the composite skins. $M = 300$ mathematical layers and order $N = 3$ for the exponential matrix are used. The no-dimensional forms of displacements and stresses are:

$$\{\bar{u}, \bar{v}, \bar{w}\} = \frac{10^6 E_2 \{u, v, w\}}{P_\beta^t h (R_\alpha/h)^4}, \quad \{\bar{\sigma}_{\alpha\alpha}, \bar{\sigma}_{\beta\beta}, \bar{\sigma}_{\alpha\beta}\} = \frac{10^5 \{\sigma_{\alpha\alpha}, \sigma_{\beta\beta}, \sigma_{\alpha\beta}\}}{P_\beta^t (R_\alpha/h)^2}, \quad (44)$$

$$\{\bar{\sigma}_{zz}, \bar{\sigma}_{\alpha z}\} = \frac{10^5 \{\sigma_{zz}, \sigma_{\alpha z}\}}{P_\beta^t (R_\alpha/h)}, \quad \bar{\sigma}_{\beta z} = \sigma_{\beta z}.$$

Results in Table 3 propose the three displacement amplitudes and the six stress amplitudes in no-dimensional form given for different positions through the thickness direction z . Results consider very thick and very thin cylinders (from $R_\alpha/h = 2$ to $R_\alpha/h = 500$). Displacements and stresses are proposed at the external surfaces ($z = +h/2$ and $z = -h/2$) and at the interface between the two composite layers ($z = 0^+$ and $z = 0^-$). Displacements and transverse shear and transverse normal stresses are continuous. On the contrary, normal in-plane and shear in-plane stresses are discontinuous at this interface. New refined 2D models must satisfy results in Table 3 in order to show a satisfactory 3D description of the proposed composite cylinder. The graphical form of these results for a very thick composite cylinder ($R_\alpha/h = 4$) is proposed in the third image of Figure 6 for the three displacement components and in Figure 9 for the six stress components. The three displacement components have a complicated evaluation through the thickness and they do not have any symmetry because the cylinder is very thick, two composite layers are included with fibre orientation $0^\circ/90^\circ$, a radius of curvature is different from infinite and load conditions are very particular. However, each displacement component is continuous at the interface between the first and the second layer because the compatibility conditions have been treated in a rigorous way. In-plane normal stresses $\bar{\sigma}_{\alpha\alpha}$ and $\bar{\sigma}_{\beta\beta}$ are discontinuous at the interface and their behavior through the thickness direction is different because there are not any symmetrical conditions for the geometry, the material and the load applications. In-plane shear stress $\bar{\sigma}_{\alpha\beta}$ is continuous because the interface is positioned between two identical composite layers where only the fibre orientation changes. Transverse normal and transverse shear stresses $\bar{\sigma}_{zz}$, $\bar{\sigma}_{\alpha z}$ and $\bar{\sigma}_{\beta z}$ are continuous because the equilibrium conditions have been opportunely included in the 3D shell model. Stresses $\bar{\sigma}_{zz}$ and $\bar{\sigma}_{\alpha z}$ are zero at the external surfaces because they satisfy the load boundary conditions in terms of amplitudes P_z and P_α , respectively. Stress $\bar{\sigma}_{\beta z}$ satisfies the load boundary conditions which are $P_\beta^t = +1Pa$ and $P_\beta^b = -1Pa$. Stresses $\bar{\sigma}_{\beta z}$ and $\bar{\sigma}_{\alpha z}$ are different because the geometry is not symmetric, the two layers have fibre orientation $0^\circ/90^\circ$ and the load conditions are not symmetric.

The fourth benchmark (B4 in Figure 4) investigates a simply supported composite cylindrical shell panel. The transverse shear load is $P_\beta^t = 1Pa$ at the top and zero at the bottom ($P_\beta^b = 0Pa$) with half-wave numbers $m = n = 1$. The radii of curvature are $R_\alpha = 10m$ and $R_\beta = \infty$. The dimensions are $a = \frac{\pi}{3}R_\alpha$ and $b = 20m$. The investigated thickness ratios are $R_\alpha/h = 2, 4, 10, 50, 100, 500$. The three layers have the same thickness ($h_1 = h_2 = h_3 = h/3$) with lamination sequence $0^\circ/90^\circ/0^\circ$. The composite material is the same already seen in the benchmark 3 and in the benchmark 2 for the external skins. $M = 300$ mathematical layers and order $N = 3$ for the exponential matrix are used. The displacements and stresses are given in the following no-dimensional forms:

$$\{\bar{u}, \bar{v}, \bar{w}\} = \frac{10^6 E_2 \{u, v, w\}}{P_\beta^t h (R_\alpha/h)^4}, \quad \{\bar{\sigma}_{\alpha\alpha}, \bar{\sigma}_{\beta\beta}, \bar{\sigma}_{\alpha\beta}\} = \frac{10^5 \{\sigma_{\alpha\alpha}, \sigma_{\beta\beta}, \sigma_{\alpha\beta}\}}{P_\beta^t (R_\alpha/h)^2}, \quad (45)$$

$$\{\bar{\sigma}_{zz}, \bar{\sigma}_{\alpha z}\} = \frac{10^5 \{\sigma_{zz}, \sigma_{\alpha z}\}}{P_\beta^t (R_\alpha/h)}, \quad \bar{\sigma}_{\beta z} = \sigma_{\beta z}.$$

Results are given in details in Table 4 where several thickness ratios are investigated (from $R_\alpha/h = 2$ to $R_\alpha/h = 500$) and different positions through the thickness direction z are proposed. Displacement amplitudes and stress amplitudes in no-dimensional form are proposed. The benchmark will allow to confirm the 3D capabilities of the new proposed refined 2D models in the case of static analysis of multilayered composite cylindrical shell panels. The fourth image in Figure 6 proposes the three displacement components for the thickness ratio $R_\alpha/h = 4$ (very thick shell). The three displacement components are continuous through the two proposed interfaces and they do not have any symmetry due to the non-symmetric geometry and load conditions. On the contrary, the lamination $0^\circ/90^\circ/0^\circ$ is symmetric through the thickness direction. The displacement behavior through the thickness direction confirms the correct imposition of compatibility conditions in the proposed 3D shell model. The six stress components are proposed for the same thickness ratio ($R_\alpha/h = 4$) in Figure 10. The in-plane

stress components $\bar{\sigma}_{\alpha\alpha}$ and $\bar{\sigma}_{\beta\beta}$ are discontinuous at each interface and they are not coincident because there is not any symmetry from the geometrical and load condition point of view. The shear in-plane stress $\bar{\sigma}_{\alpha\beta}$ is continuous at the two proposed interfaces because the three layers are made of the same composite material and the only difference is due to the fibre orientation. Transverse normal and transverse shear stresses $\bar{\sigma}_{zz}$, $\bar{\sigma}_{\alpha z}$ and $\bar{\sigma}_{\beta z}$ are continuous at each interface because equilibrium conditions have been opportunely imposed in the proposed 3D shell model. Stresses $\bar{\sigma}_{zz}$ and $\bar{\sigma}_{\alpha z}$ are zero at the external surfaces because they fulfill the load boundary conditions (loads P_z and P_α equal zero at both top and bottom of the shell). The stress $\bar{\sigma}_{\beta z}$ is equal $+1Pa$ at the top because the condition $P_\alpha^t = +1Pa$ has been here imposed, and it is equal $0Pa$ at the bottom because the condition $P_\alpha^b = 0Pa$ has been here imposed. Transverse shear stresses $\bar{\sigma}_{\alpha z}$ and $\bar{\sigma}_{\beta z}$ are completely different in their behavior through the thickness direction because there is not any symmetry in terms of geometry and applied loads.

The fifth benchmark (B5 in Figure 5) considers a simply supported composite spherical shell panel. The transverse shear load is applied at top as $P_\alpha^t = 1Pa$ and at the bottom as $P_\alpha^b = 0Pa$ (with half-wave numbers $m = n = 1$). The radii of curvature are $R_\alpha = R_\beta = 10m$ and dimensions are $a = b = \frac{\pi}{3}R_\alpha$. The investigated thickness ratios are $R_\alpha/h = 2, 4, 10, 50, 100, 500$. The four layers have the same thickness ($h_1 = h_2 = h_3 = h_4 = h/4$) with lamination sequence $0^\circ/90^\circ/0^\circ/90^\circ$. The composite material is the same already seen in the benchmarks 2, 3 and 4. $M = 300$ mathematical layers and order $N = 3$ for the exponential matrix have been set. The displacements and stresses are given in the following no-dimensional forms:

$$\{\bar{u}, \bar{v}, \bar{w}\} = \frac{10^6 E_2 \{u, v, w\}}{P_\alpha^t h (R_\alpha/h)^4}, \quad \{\bar{\sigma}_{\alpha\alpha}, \bar{\sigma}_{\beta\beta}, \bar{\sigma}_{\alpha\beta}\} = \frac{10^5 \{\sigma_{\alpha\alpha}, \sigma_{\beta\beta}, \sigma_{\alpha\beta}\}}{P_\alpha^t (R_\alpha/h)^2}, \quad (46)$$

$$\{\bar{\sigma}_{zz}, \bar{\sigma}_{\beta z}\} = \frac{10^5 \{\sigma_{zz}, \sigma_{\beta z}\}}{P_\alpha^t (R_\alpha/h)}, \quad \bar{\sigma}_{\alpha z} = \sigma_{\alpha z}.$$

No-dimensional displacement amplitudes and no-dimensional stress amplitudes at different thickness positions are proposed in numerical form in Table 5 for very thick spherical shells and very thin spherical shells (thickness ratios from $R_\alpha/h = 2$ to $R_\alpha/h = 500$). The proposed benchmark is very demanding from the 3D behavior point of view because of the presence of two radii of curvature different from infinite ($R_\alpha = R_\beta = 10m$) and because of the non-symmetrical lamination sequence ($0^\circ/90^\circ/0^\circ/90^\circ$). New refined 2D shell models proposed in the literature must give these results if they will be correctly developed and implemented. Such complicated 3D behavior is confirmed by the fifth image of Figure 6 which proposes the three displacement components through the thickness direction of a very thick shell ($R_\alpha/h = 4$). The three displacement components are continuous at each interface because of the correct implementation of the compatibility conditions in the 3D shell model. No symmetries are shown because of the particular load conditions and the non-symmetric lamination. The six stress components are given in Figure 11 for a thickness ratio $R_\alpha/h = 4$. In-plane normal stresses $\bar{\sigma}_{\alpha\alpha}$ and $\bar{\sigma}_{\beta\beta}$ are discontinuous at each interface while in-plane shear stress $\bar{\sigma}_{\alpha\beta}$ is continuous at each interface because the four layers are made of the same material and the only difference is given by the change of the fiber orientation (from 0° to 90°). Stresses $\bar{\sigma}_{\alpha\alpha}$ and $\bar{\sigma}_{\beta\beta}$ are different as behavior though the thickness, even if the spherical shell geometry is symmetric, because the lamination sequence and the load conditions are not symmetric. Transverse normal and transverse shear stresses $\bar{\sigma}_{zz}$, $\bar{\sigma}_{\alpha z}$ and $\bar{\sigma}_{\beta z}$ are continuous at each interface because equilibrium conditions have been rigorously imposed in the 3D exact shell model. $\bar{\sigma}_{zz}$ and $\bar{\sigma}_{\beta z}$ are zero at the external surfaces in order to satisfy the external boundary load conditions given for the loads P_z and P_β , respectively. Stress $\bar{\sigma}_{\alpha z}$ is zero at the bottom where $P_\alpha^b = 0Pa$ and it is $1Pa$ at the top where $P_\alpha^t = +1Pa$. Stresses $\bar{\sigma}_{\alpha z}$ and $\bar{\sigma}_{\beta z}$ are completely different even if the spherical shell has a symmetric geometry because the lamination sequence and load conditions are not symmetric.

4 Conclusions

Typical aerospace structures can be investigated as plate and shell geometries embedding sandwich or multilayered composite configurations. 3D exact shell and plate models proposed in the literature usually consider the typical load configuration which has an harmonic transverse normal load applied at the top or at the bottom of the structure. The proposed new shell model considers different combinations of loads at the external surfaces including the possibility of transverse shear loads in α and β directions in addition to the typical transverse normal load in the z direction. These three directions for the load application are combined in different ways at the top and bottom in order to obtain new results. The proposed model has already been developed for the application of transverse normal loads in harmonic form and it has been here extended to the cases of transverse shear loads opportunely modifying the imposition of the load boundary conditions in the model. Such conditions are directly imposed as opportune values of stress components $\bar{\sigma}_{zz}$, $\bar{\sigma}_{\alpha z}$ and $\bar{\sigma}_{\beta z}$ at the top and at the bottom of the structure. The model is based on the 3D differential equations of equilibrium written in general orthogonal curvilinear coordinates and it is solved using the exponential matrix method and the layer wise approach. The proposed benchmarks consider square and rectangular plates, cylinders, cylindrical and spherical shell panels. Different combinations of transverse shear and transverse normal loads simultaneously applied at the top and at the bottom of the structures have been investigated considering sandwich and laminate configurations and different thickness ratios. The 3D behavior of such structures has been proposed in terms of the three displacement components and the six stress components through different thickness positions. Compatibility and equilibrium conditions for displacements and transverse shear/normal stresses, respectively, have been discussed for each benchmark. Several considerations have been proposed for the satisfaction of the load boundary conditions. The typical zigzag form of multilayered structures has been remarked for each proposed case. The symmetry in terms of geometry, lamination sequence and load applications has been discussed for displacements and stresses in each investigated benchmark. This new 3D shell model will allow the complete validation of the new refined 2D numerical and exact plate/shell models proposed in the literature because it gives the possibility to perform several comparisons changing the geometry of the structure, the material of the embedded layers, the lamination sequence, the load conditions and the thickness ratio.

References

- [1] J.N. Reddy, *Mechanics of Laminated Composite Plates and Shells. Theory and Analysis*, CRC Press, New York, 2004.
- [2] S.W. Tsai, *Composites Design*, Think Composites, Dayton, OH, 1987.
- [3] S.W. Tsai, *Theory of Composites Design*, Think Composites, Dayton, OH, 1992.
- [4] Y.C. Fung and Pin Tong, *Classical and Computational Solid Mechanics*, Advanced Series in Engineering Science - Vol.1&2, World Scientific Publishing Co. Pte. Ltd., Singapore, 2001.
- [5] A.E.H. Love, *A Treatise on the Mathematical Theory of Elasticity*, Fourth Edition, World Cambridge University Press, USA, 1959.
- [6] G. Kirchhoff, *Über das dleichgewicht und die bewegung einer elastischen scheibe*, *Journal für Reine und Angewandte Mathematik*, 40, 51-88, 1850.
- [7] E. Reissner, *The effect of transverse shear deformation on the bending of elastic plates*, *Journal of Applied Mechanics*, 12, 69-77, 1945.

- [8] R.D. Mindlin, Influence of rotatory inertia and shear in flexural motions of isotropic elastic plates, *Journal of Applied Mechanics*, 18, 31-38, 1951.
- [9] T.S. Plagianakos and E.G. Papadopoulos, Coupled higher-order layerwise mechanics and finite element for cylindrical composite and sandwich shells with piezoelectric transducers, *European Journal of Mechanics A-Solids*, 54, 11-23, 2015.
- [10] F. Tornabene, N. Fantuzzi, M. Baccocchi and E. Viola, *Laminated Composite Doubly-Curved Shell Structures. Differential Geometry, Higher-order Structural Theories*, Vol.1, Società Editrice Esculapio, Bologna (Italy), 2016.
- [11] N.J. Pagano, Exact solutions for composite laminates in cylindrical bending, *Journal of Composite Materials*, 3, 398-411, 1969.
- [12] N.J. Pagano, Exact solutions for rectangular bidirectional composites and sandwich plates, *Journal of Composite Materials*, 4, 20-34, 1970.
- [13] N.J. Pagano and A.S.D. Wang, Further study of composite laminates under cylindrical bending, *Journal of Composite Materials*, 5, 521-528, 1971.
- [14] Y. Xu and D. Zhou, Three-dimensional elasticity solution of functionally graded rectangular plates with variable thickness, *Composite Structures*, 91, 56-65, 2009.
- [15] H.-R. Meyer-Piening, Application of the elasticity solution to linear sandwich beam, plate and shell analyses, *Journal of Sandwich Structures and Materials*, 6, 295-312, 2004.
- [16] L. Demasi, Three-dimensional closed form solutions and exact thin plate theories for isotropic plates, *Composite Structures*, 80, 183-195, 2007.
- [17] J.G. Ren, Exact solutions for laminated cylindrical shells in cylindrical bending, *Composite Science and Technology*, 29, 169-187, 1987.
- [18] T.K. Varadan and K. Bhaskar, Bending of laminated orthotropic cylindrical shells - an elasticity approach, *Composite Structures*, 17, 141-156, 1991.
- [19] J.-R. Fan and J.-Y. Zhang, Exact solutions for thick laminated shells, *Science in China*, 35, 1343-1355, 1992.
- [20] J.-R. Fan and J.-Y. Zhang, Analytical solutions for thick, doubly curved, laminated shells, *Journal of Engineering Mechanics*, 118, 1338-1356, 1992.
- [21] K.P. Soldatos and J. Ye, Axisymmetric static and dynamic analysis of laminated hollow cylinders composed of monoclinic elastic layers, *Journal of Sound and Vibration*, 184, 245-259, 1995.
- [22] J.-R. Fan and J. Ye, An exact solution for the statics and dynamics of laminated thick plates with orthotropic layers, *International Journal of Solids and Structures*, 26, 655-662, 1990.
- [23] M. Kashtalyan, Three-dimensional elasticity solution for bending of functionally graded rectangular plates, *European Journal of Mechanics - A/Solids*, 23, 853-864, 2004.
- [24] M. Kashtalyan and M. Menshykova, Three-dimensional elasticity solution for sandwich panels with a functionally graded core, *Composite Structures*, 87, 36-43, 2009.
- [25] S.S. Vel and R.C. Batra, Three-dimensional exact solution for the vibration of functionally graded rectangular plates, *Journal of Sound and Vibration*, 172, 703-730, 2004.

- [26] S. Srinivas, A.K. Rao and C.V.J. Rao, Flexure of simply supported thick homogeneous and laminated rectangular plates, *Zeitschrift für Angewandte Mathematik und Mechanik*, 49, 449-458, 1969.
- [27] A. Messina, Three dimensional free vibration analysis of cross-ply laminated plates through 2D and exact models, *3rd International Conference on Integrity, Reliability and Failure*, Porto (Portugal), 20-24 July 2009.
- [28] Q. Li, V.P. Iu and K.P. Kou, Three-dimensional vibration analysis of functionally graded material sandwich plates, *Journal of Sound and Vibration*, 311, 498-515, 2008.
- [29] A.E. Armenakas, D.C. Gazis and G. Herrmann, *Free Vibrations of Circular Cylindrical Shells*, Pergamon Press, Oxford, 1969.
- [30] N.N. Huang, Exact analysis for three-dimensional free vibrations of cross-ply cylindrical and doubly-curved laminates, *Acta Mechanica*, 108, 23-34, 1995.
- [31] P. Zahedinejad, P. Malekzadeh, M. Farid and G. Karami, A semi-analytical three-dimensional free vibration analysis of functionally graded curved panels, *International Journal of Pressure Vessels and Piping*, 87, 470-480, 2010.
- [32] P. Malekzadeh, A.R. Fiouz and H. Razi, Three-dimensional dynamic analysis of laminated composite plates subjected to moving load, *Composite Structures*, 90, 105-114, 2009.
- [33] P. Malekzadeh, A. Afsari, P. Zahedinejad and R. Bahadori, Three-dimensional layerwise-finite element free vibration analysis of thick laminated annular plates on elastic foundation, *Applied Mathematical Modelling*, 34, 776-790, 2010.
- [34] P. Malekzadeh, H. Monfared Maharloei and A.R. Vosoughi, A three-dimensional layerwise-differential quadrature free vibration of thick skew laminated composite plates, *Mechanics of Advanced Materials and Structures*, 21, 792-801, 2014.
- [35] P. Malekzadeh and M. Ghaedsharaf, Three-dimensional free vibration of laminated cylindrical panels with functionally graded layers, *Composite Structures*, 108, 894-904, 2014.
- [36] P. Malekzadeh and M. Ghaedsharaf, Three-dimensional thermoelastic analysis of finite length laminated cylindrical panels with functionally graded layers, *Meccanica*, 49, 887-906, 2014.
- [37] P. Malekzadeh and Y. Heydarpour, Mixed Navier-layerwise differential quadrature three-dimensional static and free vibration analysis of functionally graded carbon nanotube reinforced composite laminated plates, *Meccanica*, 50, 143-167, 2015.
- [38] S. Brischetto, Three-dimensional exact free vibration analysis of spherical, cylindrical, and flat one-layered panels, *Shock and Vibration*, vol.2014, 1-29, 2014.
- [39] S. Brischetto, An exact 3D solution for free vibrations of multilayered cross-ply composite and sandwich plates and shells, *International Journal of Applied Mechanics*, 6, 1-42, 2014.
- [40] S. Brischetto, Exact elasticity solution for natural frequencies of functionally graded simply-supported structures, *Computer Modeling in Engineering & Sciences*, 95, 391-430, 2013.
- [41] S. Brischetto, A continuum elastic three-dimensional model for natural frequencies of single-walled carbon nanotubes, *Composites part B: engineering*, 61, 222-228, 2014.

- [42] S. Brischetto, A continuum shell model including van der Waals interaction for free vibrations of double-walled carbon nanotubes, *Computer Modeling in Engineering & Sciences*, 104, 305-327, 2015.
- [43] S. Brischetto, Convergence analysis of the exponential matrix method for the solution of 3D equilibrium equations for free vibration analysis of plates and shells, *Composites part B: engineering*, 98, 453-471, 2016.
- [44] S. Brischetto, Exact and approximate shell geometry in the free vibration analysis of one-layered and multilayered structures, *International Journal of Mechanical Sciences*, 113, 81-93, 2016.
- [45] S. Brischetto, Curvature approximation effects in the free vibration analysis of functionally graded shells, *International Journal of Applied Mechanics*, 8, 1-33, 2016.
- [46] S. Brischetto and R. Torre, Exact 3D solutions and finite element 2D models for free vibration analysis of plates and cylinders, *Curved and Layered Structures*, 1, 59-92, 2014.
- [47] F. Tornabene, S. Brischetto, N. Fantuzzi and E. Viola, Numerical and exact models for free vibration analysis of cylindrical and spherical shell panels, *Composites part B: engineering*, 81, 231-250, 2015.
- [48] S. Brischetto, F. Tornabene, N. Fantuzzi and M. Baccocchi, Refined 2D and exact 3D shell models for the free vibration analysis of single- and double-walled carbon nanotubes, *Technologies*, 3, 259-284, 2015.
- [49] S. Brischetto, F. Tornabene, N. Fantuzzi and E. Viola, 3D exact and 2D generalized differential quadrature models for free vibration analysis of functionally graded plates and cylinders, *Meccanica*, 51, 2059-2098, 2016.
- [50] N. Fantuzzi, S. Brischetto, F. Tornabene and E. Viola, 2D and 3D shell models for the free vibration investigation of functionally graded cylindrical and spherical panels, *Composite Structures*, 154, 573-590, 2016.
- [51] S. Brischetto, F. Tornabene, N. Fantuzzi and M. Baccocchi, Interpretation of boundary conditions in the analytical and numerical shell solutions for mode analysis of multilayered structures, *International Journal of Mechanical Sciences*, 122, 18-28, 2017.
- [52] F. Tornabene, S. Brischetto, N. Fantuzzi and M. Baccocchi, Boundary conditions in 2D numerical and 3D exact models for cylindrical bending analysis of functionally graded structures, *Shock and Vibration*, vol.2016, 1-17, 2016.
- [53] S. Brischetto, Exact three-dimensional static analysis of single- and multi-layered plates and shells, *Composites Part B: Engineering*, 119, 230-252, 2017.
- [54] S. Brischetto, A general exact elastic shell solution for bending analysis of functionally graded structures, *Composite Structures*, 175, 70-85, 2017.
- [55] A.W. Leissa, *Vibration of Plates*, NASA SP-160, Washington, 1969.
- [56] A.W. Leissa, *Vibration of Shells*, NASA SP-288, Washington, 1973.
- [57] W. Soedel, *Vibration of Shells and Plates*, Marcel Dekker, Inc., New York, 2004.
- [58] F.B. Hildebrand, E. Reissner and G.B. Thomas, *Notes on the Foundations of the Theory of Small Displacements of Orthotropic Shells*, NACA Technical Note No. 1833, Washington, 1949.

- [59] F. Tornabene, *Meccanica delle Strutture a Guscio in Materiale Composito*, Società Editrice Esculapio, Bologna (Italy), 2012.
- [60] Open document, *Systems of Differential Equations*, free available on <http://www.math.utah.edu/gustafso/>, accessed on 30th May 2013.
- [61] W.E. Boyce and R.C. DiPrima, *Elementary Differential Equations and Boundary Value Problems*, John Wiley & Sons, Ltd., New York, 2001.
- [62] D. Zwillinger, *Handbook of Differential Equations*, Academic Press, New York, 1997.
- [63] C. Molery and C. Van Loan, Nineteen dubious ways to compute the exponential of a matrix, twenty-five years later, *SIAM Review*, 45, 1-46, 2003.

(α, β)	\bar{u} $(0, \frac{b}{2})$	\bar{v} $(\frac{a}{2}, 0)$	\bar{w} $(\frac{a}{2}, \frac{b}{2})$	$\bar{\sigma}_{\alpha\alpha}$ $(\frac{a}{2}, \frac{b}{2})$	$\bar{\sigma}_{\beta\beta}$ $(\frac{a}{2}, \frac{b}{2})$	$\bar{\sigma}_{\alpha\beta}$ $(0, 0)$	$\bar{\sigma}_{zz}$ $(\frac{a}{2}, \frac{b}{2})$	$\bar{\sigma}_{\alpha z}$ $(0, \frac{b}{2})$	$\bar{\sigma}_{\beta z}$ $(\frac{a}{2}, 0)$
a/h=2									
$z = -h/2$	-116.78	-116.78	-1461.2	10.590	10.590	-5.6445	1.0000	0.0000	0.0000
$z = -h/4$	88.998	88.998	-1357.0	0.0182	0.0182	0.0101	0.2729	-0.1721	-0.1721
$z = 0$	0.0000	0.0000	-1286.1	0.0000	0.0000	0.0000	0.0000	-0.1744	-0.1744
$z = +h/4$	-88.998	-88.998	-1357.0	-0.0182	-0.0182	-0.0101	-0.2729	-0.1721	-0.1721
$z = +h/2$	116.78	116.78	-1461.2	-10.590	-10.590	5.6445	-1.0000	0.0000	0.0000
a/h=4									
$z = -h/2$	-25.546	-25.546	-573.10	4.6128	4.6128	-2.4694	1.0000	0.0000	0.0000
$z = -h/4$	13.334	13.334	-563.24	0.0098	0.0098	0.0030	0.4453	-0.2818	-0.2818
$z = 0$	0.0000	0.0000	-556.66	0.0000	0.0000	0.0000	0.0000	-0.2843	-0.2843
$z = +h/4$	-13.334	-13.334	-563.24	-0.0098	-0.0098	-0.0030	-0.4453	-0.2818	-0.2818
$z = +h/2$	25.546	25.546	-573.10	-4.6128	-4.6128	2.4694	-1.0000	0.0000	0.0000
a/h=10									
$z = -h/2$	-3.3967	-3.3967	-117.78	1.5287	1.5287	-0.8209	1.0000	0.0000	0.0000
$z = -h/4$	0.2087	0.2087	-117.57	0.0029	0.0029	0.0001	0.5334	-0.3389	-0.3389
$z = 0$	0.0000	0.0000	-117.41	0.0000	0.0000	0.0000	0.0000	-0.3400	-0.3400
$z = +h/4$	-0.2087	-0.2087	-117.57	-0.0029	-0.0029	-0.0001	-0.5334	-0.3389	-0.3389
$z = +h/2$	3.3967	3.3967	-117.78	-1.5287	-1.5287	0.8209	-1.0000	0.0000	0.0000
a/h=20									
$z = -h/2$	-1.1048	-1.1048	-38.753	0.9927	0.9927	-0.5340	1.0000	0.0000	0.0000
$z = -h/4$	-0.3090	-0.3090	-38.759	0.0016	0.0016	-0.0003	0.5487	-0.3488	-0.3488
$z = 0$	0.0000	0.0000	-38.757	0.0000	0.0000	0.0000	0.0000	-0.3496	-0.3496
$z = +h/4$	0.3090	0.3090	-38.759	-0.0016	-0.0016	0.0003	-0.5487	-0.3488	-0.3488
$z = +h/2$	1.1048	1.1048	-38.753	-0.9927	-0.9927	0.5340	-1.0000	0.0000	0.0000
a/h=50									
$z = -h/2$	-0.3731	-0.3731	-15.856	0.8374	0.8374	-0.4508	1.0000	0.0000	0.0000
$z = -h/4$	-0.1709	-0.1709	-15.860	0.0012	0.0012	-0.0005	0.5531	-0.3517	-0.3517
$z = 0$	0.0000	0.0000	-15.861	0.0000	0.0000	0.0000	0.0000	-0.3524	-0.3524
$z = +h/4$	0.1709	0.1709	-15.860	-0.0012	-0.0012	0.0005	-0.5531	-0.3517	-0.3517
$z = +h/2$	0.3731	0.3731	-15.856	-0.8374	-0.8374	0.4508	-1.0000	0.0000	0.0000
a/h=100									
$z = -h/2$	-0.1816	-0.1816	-12.556	0.8150	0.8150	-0.4388	1.0000	0.0000	0.0000
$z = -h/4$	-0.0888	-0.0888	-12.557	0.0011	0.0011	-0.0005	0.5538	-0.3521	-0.3521
$z = 0$	0.0000	0.0000	-12.558	0.0000	0.0000	0.0000	0.0000	-0.3528	-0.3528
$z = +h/4$	0.0888	0.0888	-12.557	-0.0011	-0.0011	0.0005	-0.5538	-0.3521	-0.3521
$z = +h/2$	0.1816	0.1816	-12.556	-0.8150	-0.8150	0.4388	-1.0000	0.0000	0.0000

Table 1: Benchmark 1, 3D exact displacements and stresses for a sandwich square plate with isotropic skins.

(α, β)	\bar{u} $(0, \frac{b}{2})$	\bar{v} $(\frac{a}{2}, 0)$	\bar{w} $(\frac{a}{2}, \frac{b}{2})$	$\bar{\sigma}_{\alpha\alpha}$ $(\frac{a}{2}, \frac{b}{2})$	$\bar{\sigma}_{\beta\beta}$ $(\frac{a}{2}, \frac{b}{2})$	$\bar{\sigma}_{\alpha\beta}$ $(0, 0)$	$\bar{\sigma}_{zz}$ $(\frac{a}{2}, \frac{b}{2})$	$\bar{\sigma}_{\alpha z}$ $(0, \frac{b}{2})$	$\bar{\sigma}_{\beta z}$ $(\frac{a}{2}, 0)$
a/h=2									
$z = -h/2$	4113.8	-670.25	4085.5	-31928	-482.22	231.52	0.0000	-1.0000	0.0000
$z = -h/4$	283.58	-1600.4	2956.0	-72.091	-65.820	-5.7789	-241.92	-0.0089	-9.5391
$z = 0$	-1392.3	-2023.5	0.0677	-53.638	-59.147	-9.5462	-250.77	0.0000	0.0002
$z = +h/4$	283.60	-1600.4	-2955.9	-72.090	-65.819	-5.7788	-241.92	0.0089	9.5395
$z = +h/2$	4113.8	-670.26	-4085.4	-31928	-482.22	231.52	0.0000	1.0000	0.0000
a/h=4									
$z = -h/2$	945.81	-201.94	-32.630	-14676	-201.61	74.859	0.0000	-1.0000	0.0000
$z = -h/4$	815.33	-221.02	3.3229	-28.244	-14.598	0.3896	-61.588	-0.0086	-3.9161
$z = 0$	746.65	-233.54	0.0026	-26.859	-14.203	0.1177	-63.808	0.0000	0.0000
$z = +h/4$	815.33	-221.02	-3.3176	-28.244	-14.598	0.3896	-61.588	0.0086	3.9162
$z = +h/2$	945.81	-201.94	32.635	-14676	-201.61	74.859	0.0000	1.0000	0.0000
a/h=10									
$z = -h/2$	149.91	-31.668	-10.640	-5815.5	-80.242	30.222	0.0000	-1.0000	0.0000
$z = -h/4$	147.60	-31.798	-5.4387	-9.3238	-3.2527	0.3339	-9.7347	-0.0074	-1.1054
$z = 0$	146.31	-31.953	0.0000	-9.2616	-3.2382	0.3227	-10.038	0.0000	0.0000
$z = +h/4$	147.60	-31.798	5.4388	-9.3238	-3.2527	0.3339	-9.7347	0.0074	1.1054
$z = +h/2$	149.91	-31.668	10.640	-5815.5	-80.242	30.222	0.0000	1.0000	0.0000
a/h=20									
$z = -h/2$	37.445	-7.8758	-1.4722	-2905.3	-40.159	15.212	0.0000	-1.0000	0.0000
$z = -h/4$	37.311	-7.8806	-0.7726	-4.4983	-1.4331	0.1748	-2.4278	-0.0071	-0.5116
$z = 0$	37.235	-7.8886	0.0000	-4.4911	-1.4315	0.1736	-2.5013	0.0000	0.0000
$z = +h/4$	37.311	-7.8806	0.7726	-4.4983	-1.4331	0.1748	-2.4278	0.0071	0.5116
$z = +h/2$	37.445	-7.8758	1.4722	-2905.3	-40.159	15.212	0.0000	1.0000	0.0000
a/h=50									
$z = -h/2$	5.9899	-1.2582	-0.0967	-1161.9	-16.069	6.0974	0.0000	-1.0000	0.0000
$z = -h/4$	5.9866	-1.2583	-0.0511	-1.7806	-0.5514	0.0707	-0.3882	-0.0071	-0.1999
$z = 0$	5.9847	-1.2585	0.0000	-1.7801	-0.5513	0.0706	-0.3998	0.0000	0.0000
$z = +h/4$	5.9866	-1.2583	0.0511	-1.7806	-0.5514	0.0707	-0.3882	0.0071	0.1999
$z = +h/2$	5.9899	-1.2582	0.0967	-1161.9	-16.069	6.0974	0.0000	1.0000	0.0000
a/h=100									
$z = -h/2$	1.4974	-0.3145	-0.0121	-580.92	-8.0349	3.0496	0.0000	-1.0000	0.0000
$z = -h/4$	1.4972	-0.3145	-0.0064	-0.8889	-0.2742	0.0354	-0.0970	-0.0071	-0.0996
$z = 0$	1.4971	-0.3145	0.0000	-0.8889	-0.2741	0.0354	-0.0999	0.0000	0.0000
$z = +h/4$	1.4972	-0.3145	0.0064	-0.8889	-0.2742	0.0354	-0.0970	0.0071	0.0996
$z = +h/2$	1.4974	-0.3145	0.0121	-580.92	-8.0349	3.0496	0.0000	1.0000	0.0000

Table 2: Benchmark 2, 3D exact displacements and stresses for a sandwich rectangular plate with composite skins.

(α, β)	\bar{u} $(0, \frac{b}{2})$	\bar{v} $(\frac{a}{2}, 0)$	\bar{w} $(\frac{a}{2}, \frac{b}{2})$	$\bar{\sigma}_{\alpha\alpha}$ $(\frac{a}{2}, \frac{b}{2})$	$\bar{\sigma}_{\beta\beta}$ $(\frac{a}{2}, \frac{b}{2})$	$\bar{\sigma}_{\alpha\beta}$ $(0, 0)$	$\bar{\sigma}_{zz}$ $(\frac{a}{2}, \frac{b}{2})$	$\bar{\sigma}_{\alpha z}$ $(0, \frac{b}{2})$	$\bar{\sigma}_{\beta z}$ $(\frac{a}{2}, 0)$
$R_\alpha/h=2$									
$z = -h/2$	1212.1	58243	2548.3	-4418.1	-36681	8564.2	0.0000	0.0000	-1.0000
$z = 0^-$	558.93	5421.1	8221.4	16228	-5682.4	754.49	-10582	-1218.5	-0.2260
$z = 0^+$	558.93	5421.1	8221.4	-1911.3	-43650	754.49	-10582	-1218.5	-0.2260
$z = +h/2$	-1927.8	15118	4943.2	-1185.9	-117191	634.75	0.0000	0.0000	1.0000
$R_\alpha/h=4$									
$z = -h/2$	1070.2	7259.4	2207.8	4231.0	-9039.9	2451.2	0.0000	0.0000	-1.0000
$z = 0^-$	808.49	2063.9	2876.3	9341.4	-2767.1	967.98	-2903.6	-1207.3	-0.5106
$z = 0^+$	808.49	2063.9	2876.3	-155.17	-32132	967.98	-2903.6	-1207.3	-0.5106
$z = +h/2$	423.35	1949.2	2812.8	262.95	-30083	643.92	0.0000	0.0000	1.0000
$R_\alpha/h=10$									
$z = -h/2$	108.08	492.27	283.96	1916.3	-1509.1	450.85	0.0000	0.0000	-1.0000
$z = 0^-$	95.984	316.61	311.06	2411.0	-959.47	324.92	-241.52	-486.82	-0.7430
$z = 0^+$	95.984	316.61	311.06	-35.754	-12256	324.92	-241.52	-486.82	-0.7430
$z = +h/2$	81.435	281.60	320.35	15.289	-10884	275.44	0.0000	0.0000	1.0000
$R_\alpha/h=50$									
$z = -h/2$	-1.8204	12.336	0.9928	128.96	-191.25	17.718	0.0000	0.0000	-1.0000
$z = 0^-$	-1.8512	12.082	1.1730	141.28	-186.94	16.469	9.9572	-40.667	-0.8380
$z = 0^+$	-1.8512	12.082	1.1730	-30.472	-2343.1	16.469	9.9572	-40.667	-0.8380
$z = +h/2$	-1.8845	12.056	1.2935	-29.858	-2337.9	15.812	0.0000	0.0000	1.0000
$R_\alpha/h=100$									
$z = -h/2$	-0.7061	3.0355	-0.1800	42.387	-94.535	4.3755	0.0000	0.0000	-1.0000
$z = 0^-$	-0.7089	3.0243	-0.1573	45.320	-94.092	4.1911	7.4380	-15.180	-0.8451
$z = 0^+$	-0.7089	3.0243	-0.1573	-17.332	-1173.5	4.1911	7.4380	-15.180	-0.8451
$z = +h/2$	-0.7118	3.0274	-0.1416	-17.234	-1174.7	4.0801	0.0000	0.0000	1.0000
$R_\alpha/h=500$									
$z = -h/2$	-0.0365	0.1212	-0.0213	4.8311	-18.952	0.1730	0.0000	0.0000	1.0000
$z = 0^-$	-0.0365	0.1213	-0.0211	4.9445	-18.955	0.1697	1.8620	-2.1738	-0.8498
$z = 0^+$	-0.0365	0.1213	-0.0211	-3.8175	-235.42	0.1697	1.8620	-2.1738	-0.8498
$z = +h/2$	-0.0366	0.1214	-0.0210	-3.8155	-235.55	0.1670	0.0000	0.0000	1.0000

Table 3: Benchmark 3, 3D exact displacements and stresses for a two-layered $0^\circ/90^\circ$ composite cylinder. 0^- means top of the first layer. 0^+ means bottom of the second layer.

(α, β)	\bar{u} $(0, \frac{b}{2})$	\bar{v} $(\frac{a}{2}, 0)$	\bar{w} $(\frac{a}{2}, \frac{b}{2})$	$\bar{\sigma}_{\alpha\alpha}$ $(\frac{a}{2}, \frac{b}{2})$	$\bar{\sigma}_{\beta\beta}$ $(\frac{a}{2}, \frac{b}{2})$	$\bar{\sigma}_{\alpha\beta}$ $(0, 0)$	$\bar{\sigma}_{zz}$ $(\frac{a}{2}, \frac{b}{2})$	$\bar{\sigma}_{\alpha z}$ $(0, \frac{b}{2})$	$\bar{\sigma}_{\beta z}$ $(\frac{a}{2}, 0)$
$R_\alpha/h=2$									
$z = -h/2$	-20657	-491.77	-40410	71132	1541.6	-3617.9	0.0000	0.0000	0.0000
$z = -h/4$	-14144	6399.4	-39995	6520.7	-1727.1	-29.137	637.20	-21550	-0.0275
$z = 0$	-15659	15762	-40125	-1319.0	-61987	2385.2	-6043.3	-16292	0.2318
$z = +h/4$	-14623	43265	-39744	4973.3	-14610	9714.1	-4551.5	-12321	0.7281
$z = +h/2$	-8648.8	90050	-33843	-22446	-28728	21292	0.0000	0.0000	1.0000
$R_\alpha/h=4$									
$z = -h/2$	-4819.8	2216.6	-9652.5	26836	-869.44	6.0940	0.0000	0.0000	0.0000
$z = -h/4$	-3673.7	3199.6	-9533.9	7606.5	-1528.1	939.46	2726.2	-11873	0.0334
$z = 0$	-3306.9	4436.4	-9351.8	-303.38	-34312	1706.1	1127.7	-11258	0.3926
$z = +h/4$	-2852.5	6895.1	-9112.0	-3564.8	-4318.2	3151.2	682.65	-8428.0	0.8506
$z = +h/2$	-1823.6	10445	-8643.2	-15531	-6865.7	5254.0	0.0000	0.0000	1.0000
$R_\alpha/h=10$									
$z = -h/2$	-960.48	561.23	-2138.3	9460.5	-697.10	138.56	0.0000	0.0000	0.0000
$z = -h/4$	-831.18	646.77	-2129.9	4422.3	-854.35	359.76	1537.7	-5086.0	0.0492
$z = 0$	-726.78	739.78	-2118.2	-145.63	-14302	566.49	1452.0	-5545.5	0.4481
$z = +h/4$	-621.02	865.19	-2102.2	-3173.7	-1368.0	818.28	1079.1	-4282.8	0.8919
$z = +h/2$	-494.66	1017.7	-2079.1	-7394.6	-1742.8	1120.0	0.0000	0.0000	1.0000
$R_\alpha/h=50$									
$z = -h/2$	-73.731	31.457	-203.87	1022.2	-227.13	-53.851	0.0000	0.0000	0.0000
$z = -h/4$	-71.027	33.060	-203.77	517.57	-247.71	-31.252	188.46	-594.67	0.0304
$z = 0$	-68.349	34.674	-203.67	-56.653	-3364.3	-8.7767	209.32	-683.60	0.4715
$z = +h/4$	-65.671	36.346	-203.55	-469.56	-292.98	14.031	166.82	-544.16	0.9353
$z = +h/2$	-62.972	38.059	-203.38	-957.47	-317.59	37.135	0.0000	0.0000	1.0000
$R_\alpha/h=100$									
$z = -h/2$	-18.368	8.3083	-52.700	267.40	-125.29	-19.987	0.0000	0.0000	0.0000
$z = -h/4$	-18.018	8.5154	-52.685	137.48	-130.83	-14.149	50.127	-158.62	0.0374
$z = 0$	-17.668	8.7232	-52.672	-29.437	-1693.4	-8.3209	54.782	-178.32	0.4853
$z = +h/4$	-17.318	8.9346	-52.658	-120.44	-142.48	-2.4514	42.731	-138.31	0.9449
$z = +h/2$	-16.968	9.1486	-52.639	-248.19	-148.55	3.4494	0.0000	0.0000	1.0000
$R_\alpha/h=500$									
$z = -h/2$	-0.6716	0.3388	-1.9848	12.182	-26.372	-0.9871	0.0000	0.0000	0.0000
$z = -h/4$	-0.6690	0.3404	-1.9847	7.3175	-26.587	-0.7684	2.4361	-7.6580	0.0487
$z = 0$	-0.6663	0.3419	-1.9846	-5.7488	-331.89	-0.5497	2.0627	-6.7321	0.4973
$z = +h/4$	-0.6637	0.3435	-1.9845	-2.4269	-27.024	-0.3306	1.0623	-3.5509	0.9480
$z = +h/2$	-0.6610	0.3451	-1.9843	-7.2748	-27.242	-0.1113	0.0000	0.0000	1.0000

Table 4: Benchmark 4, 3D exact displacements and stresses for a three-layered $0^\circ/90^\circ/0^\circ$ composite cylindrical shell panel.

(α, β)	\bar{u} $(0, \frac{b}{2})$	\bar{v} $(\frac{a}{2}, 0)$	\bar{w} $(\frac{a}{2}, \frac{b}{2})$	$\bar{\sigma}_{\alpha\alpha}$ $(\frac{a}{2}, \frac{b}{2})$	$\bar{\sigma}_{\beta\beta}$ $(\frac{a}{2}, \frac{b}{2})$	$\bar{\sigma}_{\alpha\beta}$ $(0, 0)$	$\bar{\sigma}_{zz}$ $(\frac{a}{2}, \frac{b}{2})$	$\bar{\sigma}_{\alpha z}$ $(0, \frac{b}{2})$	$\bar{\sigma}_{\beta z}$ $(\frac{a}{2}, 0)$
$R_\alpha/h=2$									
$z = -h/2$	-3159.9	-4610.9	-7000.2	8615.3	1990.0	-3267.7	0.0000	0.0000	0.0000
$z = -h/3$	31.941	-3079.8	-7359.4	-1906.7	4411.0	-1048.6	-1494.2	0.0051	-3790.6
$z = +h/3$	9068.2	-4483.3	-7550.6	-80548	-2485.3	1334.7	-8178.3	0.4796	-3319.2
$z = +h/2$	65840	-3902.4	-2737.1	-31846	10021	15627	0.0000	1.0000	0.0000
$R_\alpha/h=4$									
$z = -h/2$	370.34	-171.05	-66.927	-6609.5	75.101	143.66	0.0000	0.0000	0.0000
$z = -h/3$	892.23	-159.53	-58.216	-1224.2	1807.9	482.25	-963.02	0.2450	-171.54
$z = +h/3$	2080.1	-235.00	32.114	-29653	-626.58	1117.3	-2705.1	0.7013	-106.81
$z = +h/2$	5711.1	-266.06	316.53	-5911.8	3459.2	3052.9	0.0000	1.0000	0.0000
$R_\alpha/h=10$									
$z = -h/2$	371.38	241.93	600.88	-6712.4	-262.37	1018.0	0.0000	0.0000	0.0000
$z = -h/3$	347.56	191.94	605.69	-499.00	225.20	865.16	-1203.9	0.5464	1079.7
$z = +h/3$	349.55	146.76	607.92	-5365.1	-0.2471	769.81	-1234.7	0.8562	1440.5
$z = +h/2$	391.12	99.763	610.21	-467.45	3532.3	737.21	0.0000	1.0000	0.0000
$R_\alpha/h=50$									
$z = -h/2$	23.817	17.473	56.345	-938.58	1.5254	328.84	0.0000	0.0000	0.0000
$z = -h/3$	22.875	16.462	56.361	-55.086	416.60	311.19	-172.36	0.4904	214.83
$z = +h/3$	21.974	15.454	56.365	-578.15	36.903	294.12	-171.25	0.7972	264.84
$z = +h/2$	21.132	14.445	56.358	-19.462	788.75	277.73	0.0000	1.0000	0.0000
$R_\alpha/h=100$									
$z = -h/2$	6.0822	4.4308	15.033	-395.16	9.7891	166.61	0.0000	0.0000	0.0000
$z = -h/3$	5.9535	4.2951	15.034	-23.601	259.04	161.88	-68.805	0.4515	92.177
$z = +h/3$	5.8274	4.1594	15.034	-296.30	19.401	157.22	-68.735	0.7705	105.90
$z = +h/2$	5.7050	4.0238	15.034	-13.699	359.50	152.65	0.0000	1.0000	0.0000
$R_\alpha/h=500$									
$z = -h/2$	0.2456	0.1772	0.6280	-66.072	3.5396	33.366	0.0000	0.0000	0.0000
$z = -h/3$	0.2445	0.1761	0.6280	-4.1011	60.493	33.168	-10.621	0.4161	15.490
$z = +h/3$	0.2434	0.1749	0.6280	-61.874	3.9459	32.970	-10.627	0.7465	16.075
$z = +h/2$	0.2423	0.1738	0.6280	-3.6763	64.719	32.774	0.0000	1.0000	0.0000

Table 5: Benchmark 5, 3D exact displacements and stresses for a four-layered $0^\circ/90^\circ/0^\circ/90^\circ$ composite spherical shell panel.

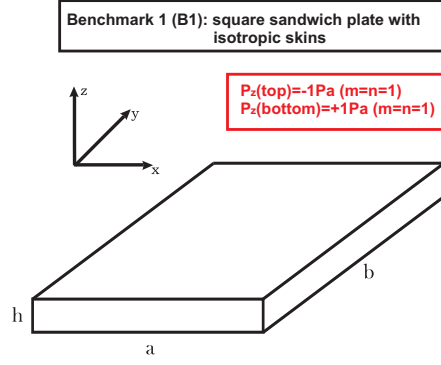


Figure 1: Geometry, lamination, materials and loads for the benchmark 1 (B1).

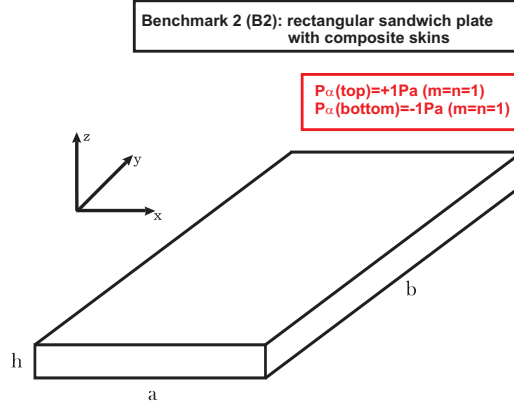


Figure 2: Geometry, lamination, materials and loads for the benchmark 2 (B2).

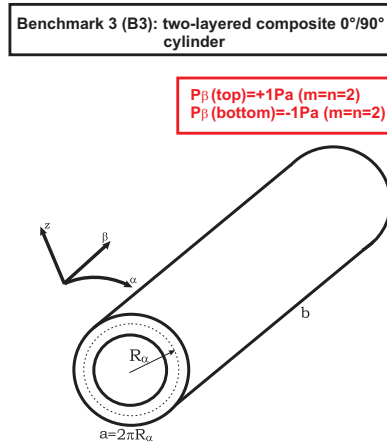


Figure 3: Geometry, lamination, materials and loads for the benchmark 3 (B3).

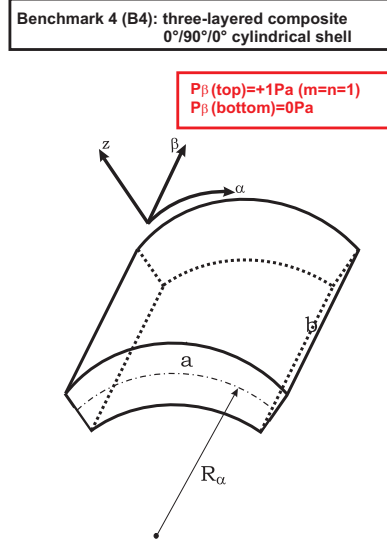


Figure 4: Geometry, lamination, materials and loads for the benchmark 4 (B4).

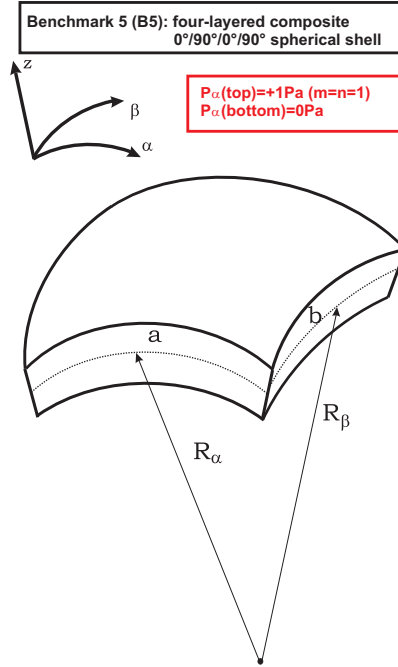


Figure 5: Geometry, lamination, materials and loads for the benchmark 5 (B5).

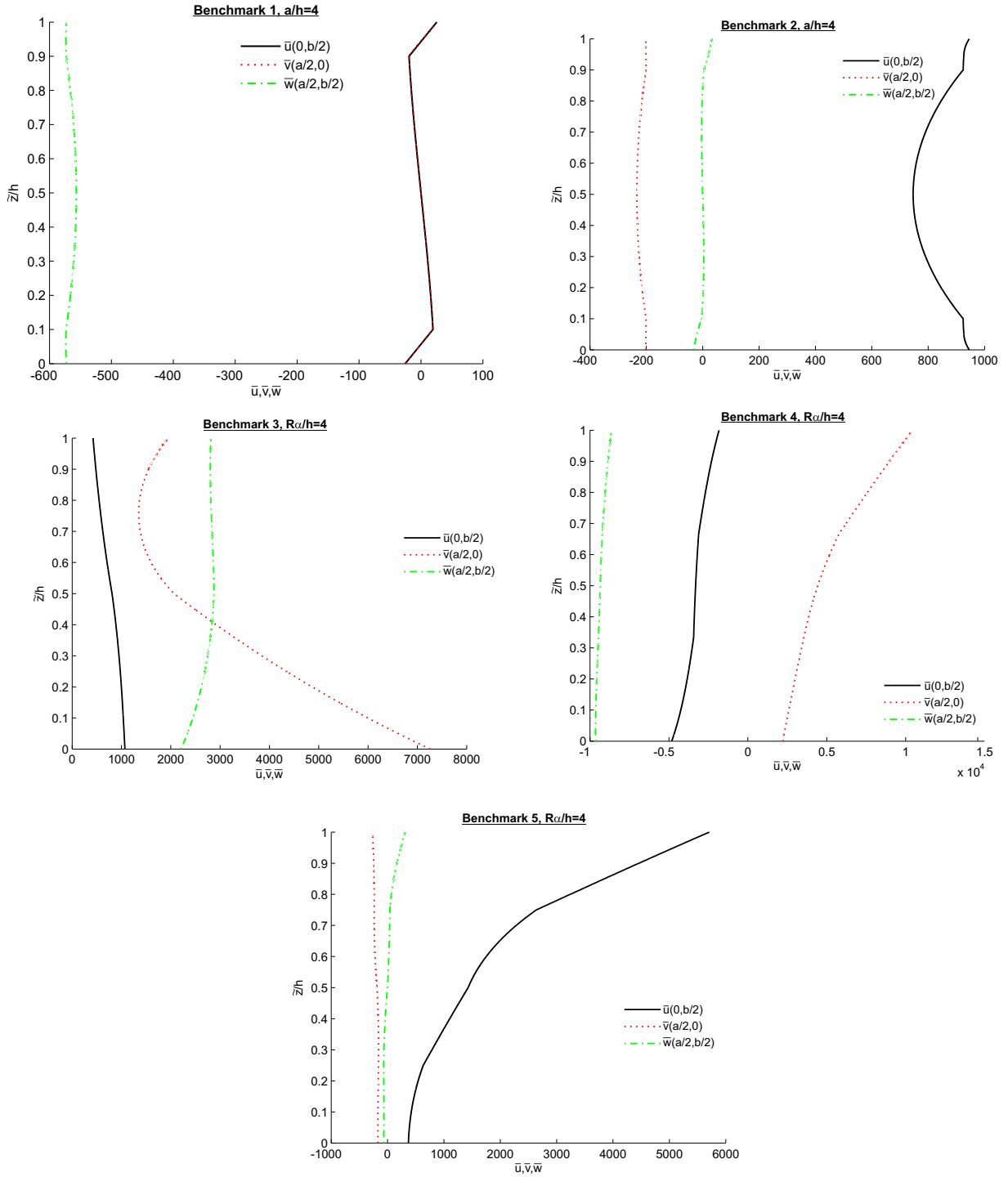


Figure 6: No-dimensional displacements through the thickness direction for the five proposed benchmarks.

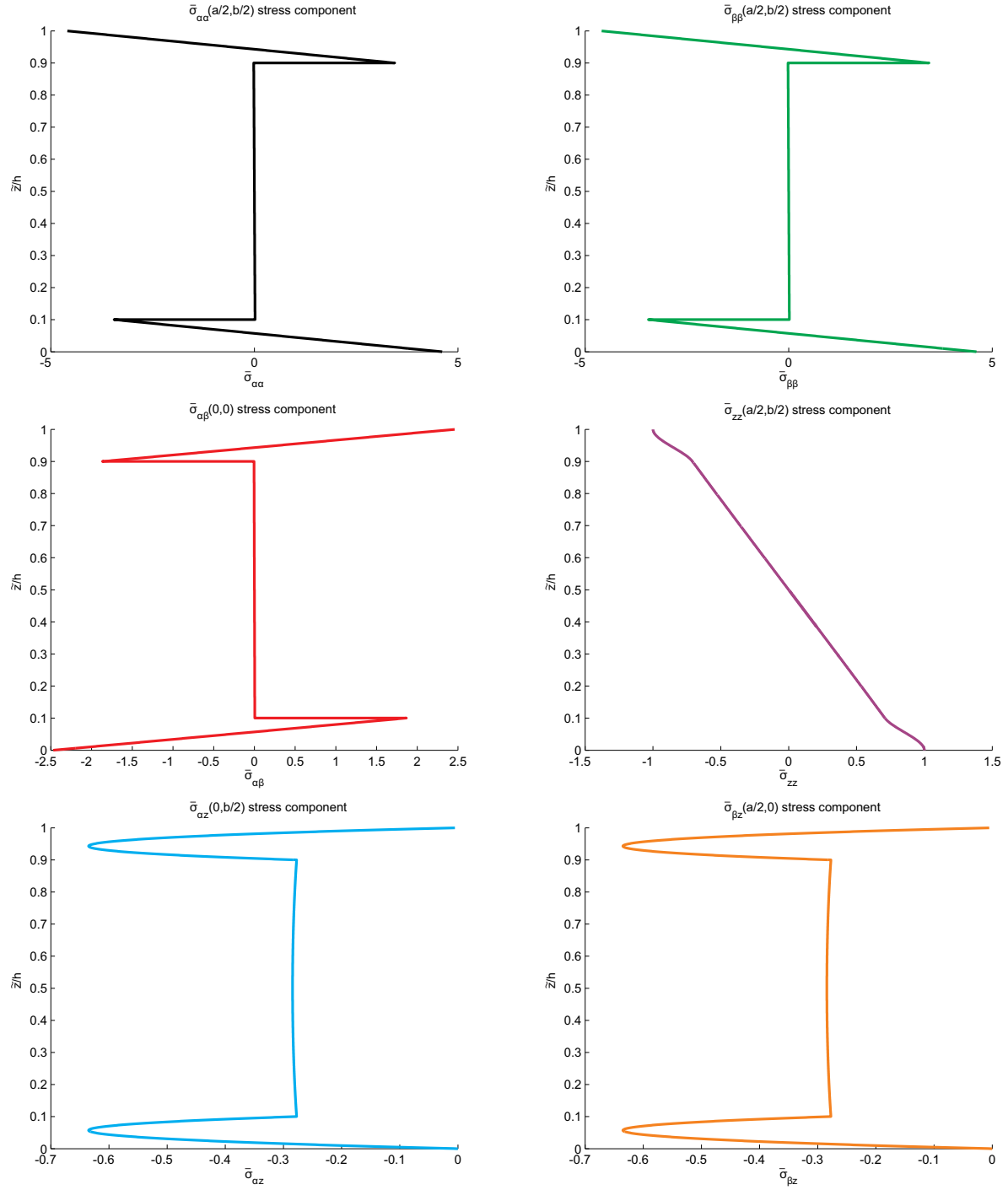


Figure 7: No-dimensional stresses through the thickness direction for the benchmark 1 (B1) about the square sandwich plate with isotropic skins ($a/h = 4$).

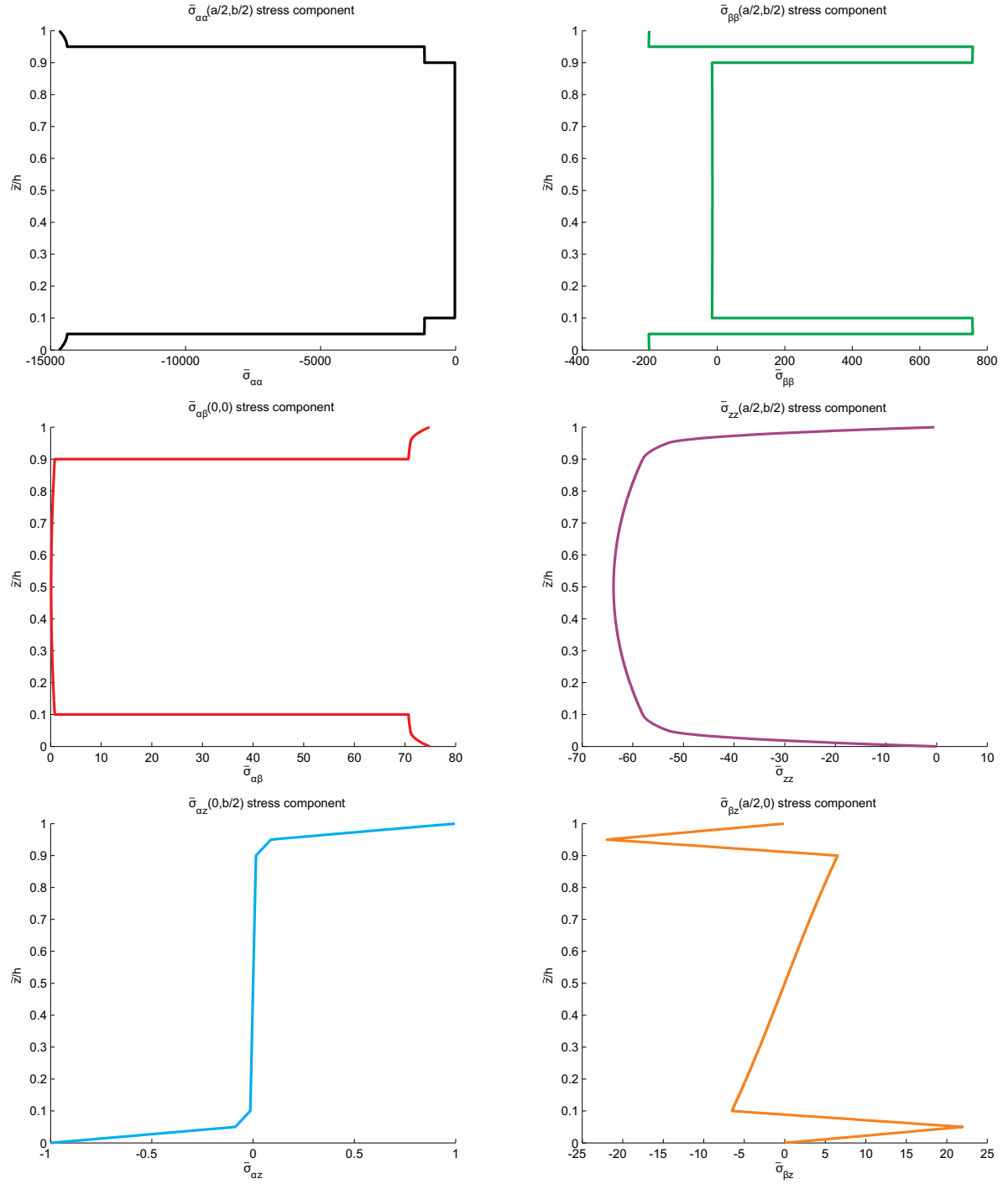


Figure 8: No-dimensional stresses through the thickness direction for the benchmark 2 (B2) about the rectangular sandwich plate with composite skins ($a/h = 4$).

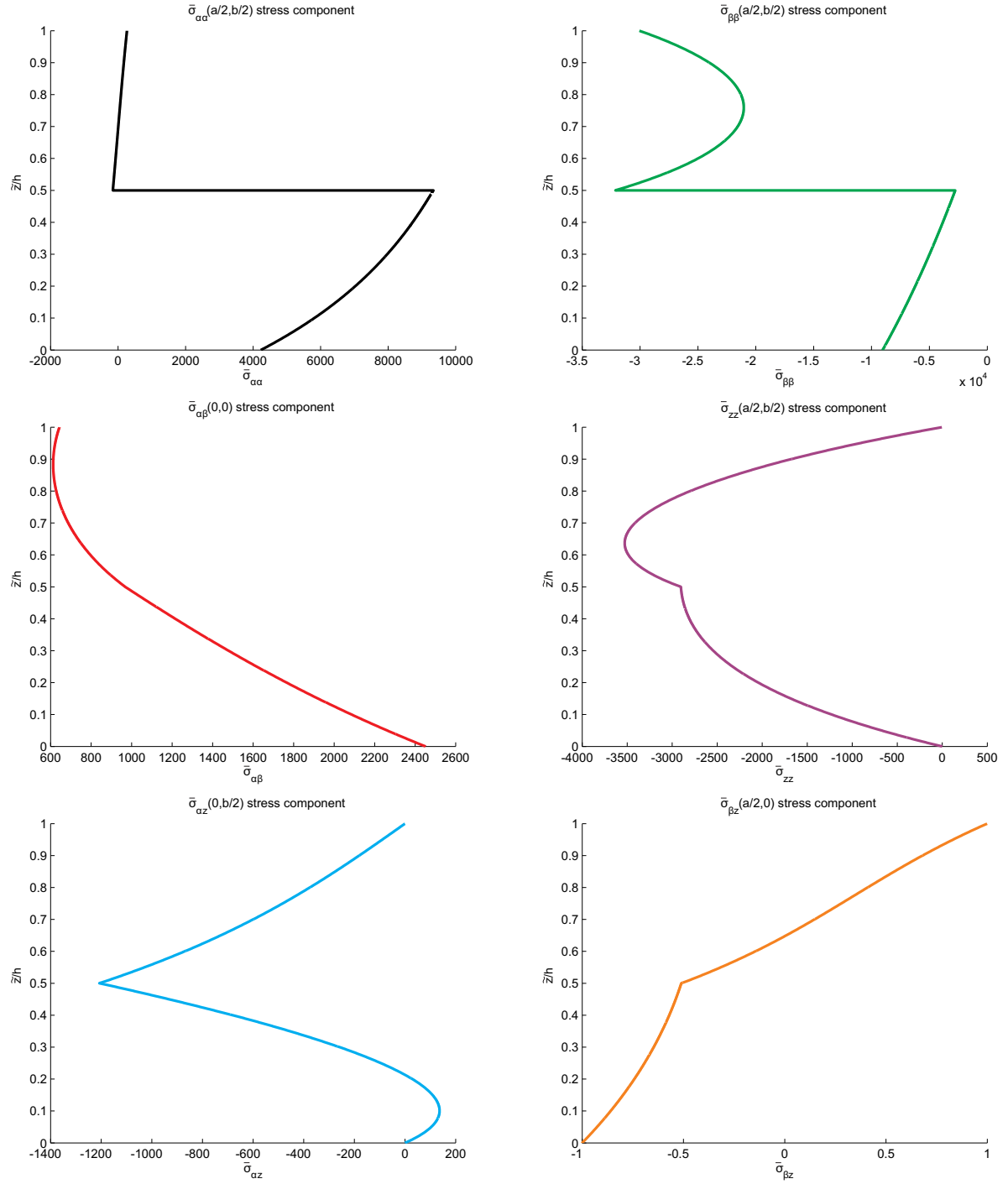


Figure 9: No-dimensional stresses through the thickness direction for the benchmark 3 (B3) about the two-layered $0^\circ/90^\circ$ composite cylinder ($R_\alpha/h = 4$).

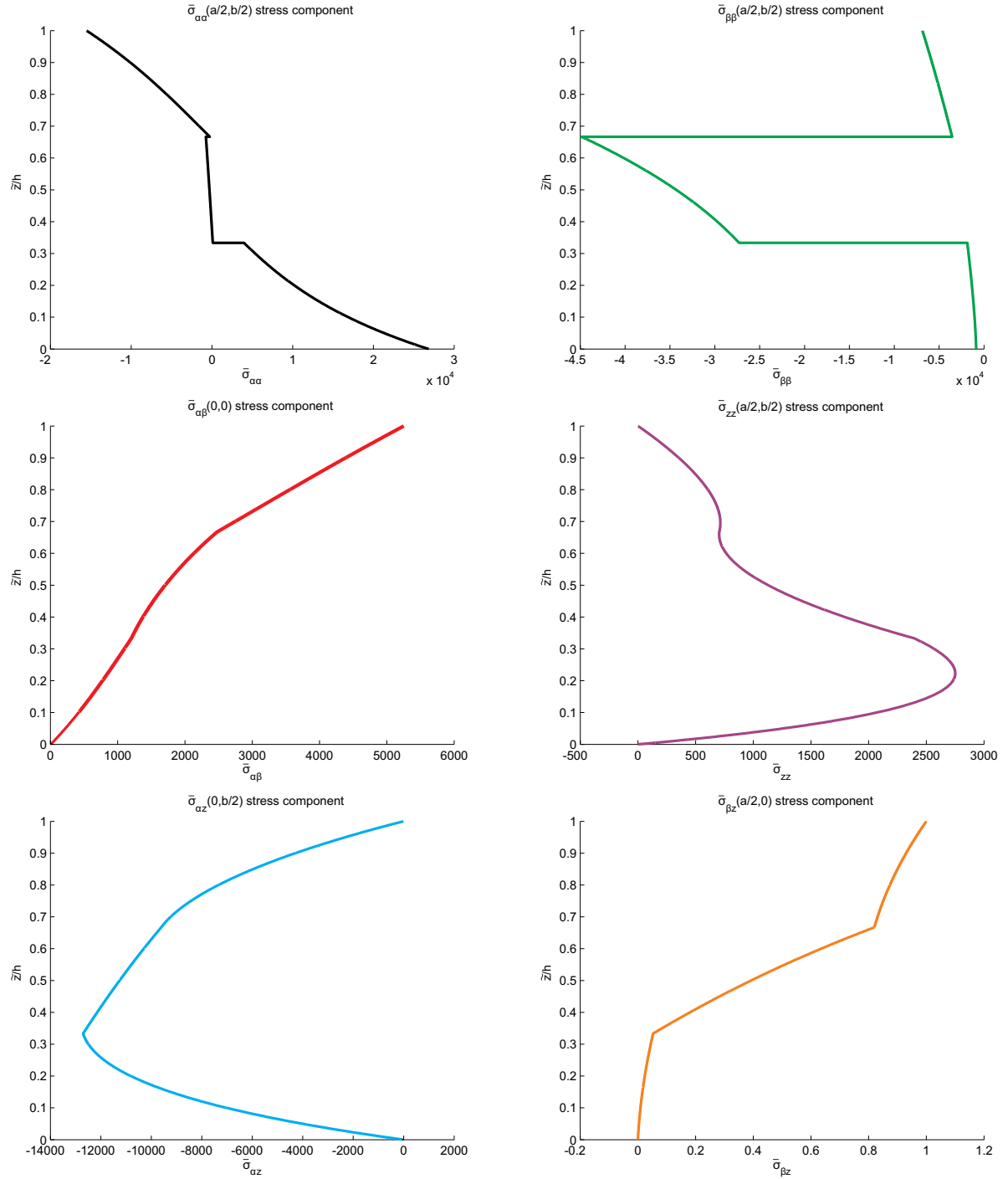


Figure 10: No-dimensional stresses through the thickness direction for the benchmark 4 (B4) about the three-layered $0^\circ/90^\circ/0^\circ$ composite cylindrical shell panel ($R_\alpha/h = 4$).

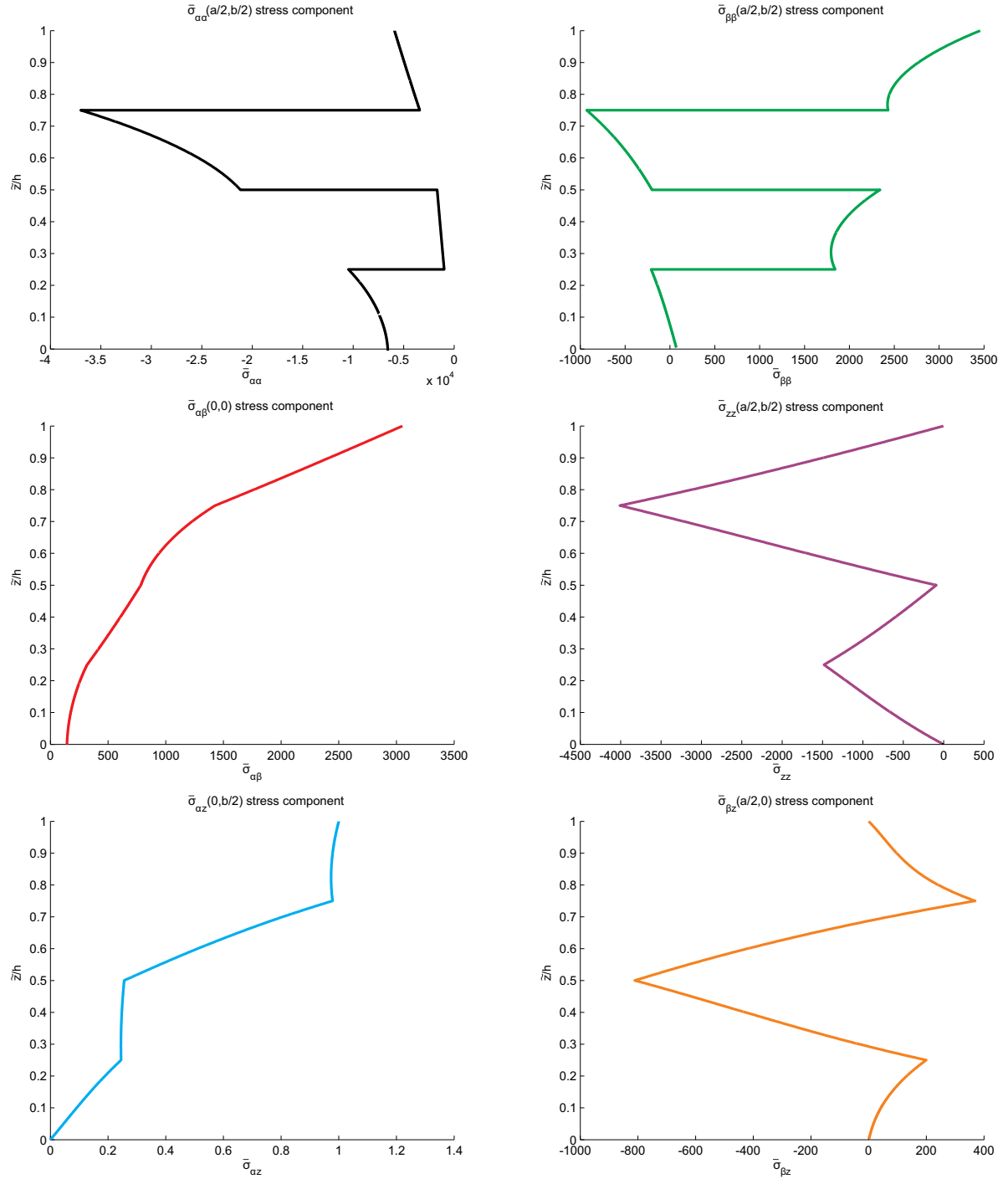


Figure 11: No-dimensional stresses through the thickness direction for the benchmark 5 (B5) about the four-layered $0^\circ/90^\circ/0^\circ/90^\circ$ composite spherical shell panel ($R_\alpha/h = 4$).